

Research paper

A synthetic circular RNA targeting miR-340-5p promotes optic nerve regeneration and retinal ganglion cell survival following axotomy



Matthew A. Hintermayer, Elizabeth M.-L. Hua, Mohammed Noor, Isabel Rambaldi,
Alyson E. Fournier*

Department of Neurology and Neurosurgery, Montréal Neurological Institute, McGill University, Montréal H3A 2B4, Canada

ARTICLE INFO

Keywords:
Axon regeneration
Neuronal survival
Neurotrauma
microRNA
Circular RNA
RNA therapeutic

ABSTRACT

The regeneration of axons in the mammalian central nervous system is severely restricted, owing to an age-dependant reduction in intrinsic regenerative capacity, a loss of neurotrophic support, and an inhibitory growth environment. In the dorsal root ganglion (DRG) conditioning lesion model, peripheral axotomy results in transcriptional reprogramming of neurons into a regenerative state, but this reprogramming involves extensive multi-gene changes that are difficult to recapitulate in non-regenerating CNS neurons. MicroRNAs are small non-coding RNAs that individually regulate groups of related genes and are attractive as tool compounds for modulating complex transcriptional changes in cells. Computational modelling was applied to single-cell RNA sequencing datasets from mice subjected to the DRG conditioning lesion paradigm, identifying individual miRNAs that target multiple regeneration associated genes (RAGs). Inhibiting miR-340-5p derepresses RAGs and promotes neurite growth *in vitro*. A circular RNA sponge designed to sequester miR-340-5p (Circ-340-5p) disinhibits RAGs in the retinal ganglion cells of male and female C57BL/6 mice, whilst simultaneously activating pro-regenerative PI3K signalling and pro-survival BDNF/TRKB signalling. Circ-340-5p enhanced post-axotomy neuronal survival acutely following ONC, but this effect was not sustained at six weeks. Circ-340-5p promoted axon regeneration and the extent of regeneration improved over time. Our findings establish an approach for recapitulating multi-gene transcriptional changes in neurons to promote axon regeneration and neuronal survival following axotomy, and outline a platform for the development of long-acting miRNA-targeting therapeutics.

1. Introduction

Following axotomy, neurons in the adult mammalian central nervous system (CNS) demonstrate a severely restricted ability to regenerate their axons, leaving individuals who sustain neurotrauma with lifelong functional impairments. This paucity of regeneration results, in part, from an age-dependant reduction in the expression of regeneration-associated genes (RAGs) that are active during embryonic development and are downregulated postnatally (Puttagunta et al., 2014; Tedeschi and Bradke, 2017). Following optic nerve crush (ONC), retinal ganglion cells (RGCs) initiate apoptotic signalling leading to neuronal loss that occurs in a predictable, time-dependant manner (Cameron et al., 2020; Daniel et al., 2018; Tran et al., 2019). Neuronal death following axotomy is in part due to a reduction or loss of neurotrophic support from downstream effector cells, which can be temporarily overcome via the facilitation of this signalling by treatment with

exogenous neurotrophins or the expression of constitutively active receptor components (Di Polo et al., 1998; Feng et al., 2017; Taniguchi et al., 2024; Vidal-Villegas et al., 2021). Effective therapeutics for axonal injury must simultaneously target molecular signalling cascades that regulate both regeneration and survival.

Experimental models permissive to CNS axon regeneration have enabled the identification of RAG programs. In pseudounipolar dorsal root ganglion (DRG) sensory neurons, a peripheral sciatic nerve lesion conditions sensory neurons to regenerate axons centrally in the spinal cord (Kadoya et al., 2009; McQuarrie and Grafstein, 1973; Neumann and Woolf, 1999). DRGs exposed to conditioning lesions also show enhanced outgrowth in explant cultures, supporting a role for neuron-intrinsic effects mediated by transcriptional reprogramming in this response (De Virgiliis et al., 2020; Niemi et al., 2022). Further, some gene manipulations that enhance growth in conditioned DRGs can also promote regeneration in CNS neurons, highlighting shared components of a core

* Corresponding author.

E-mail address: alyson.fournier@mcgill.ca (A.E. Fournier).

regenerative program. However, these single-gene modulations have shown limited success, likely reflecting the polygenic nature of the conditioning lesion response (Apara et al., 2017; Moore et al., 2009). A more refined approach has involved overexpressing regeneration-associated transcription factors like KLF6, KLF7, SMAD1, or SOX11, which can drive axon growth *in vitro* and *in vivo* (Blackmore et al., 2012; Renthal et al., 2020; Zhao et al., 2023). These effects can be constrained by developmental epigenetic barriers that limit access to key binding sites. In contrast, multi-gene modulation and combinatorial strategies tend to produce more sustained and long-distance regeneration (Benowitz and Yin, 2007; Kurimoto et al., 2010; Sun et al., 2011; Yang et al., 2020). This suggests that targeting coordinated gene programs at the post-transcriptional level may offer a more effective path to enhancing regeneration and neuronal survival.

MicroRNAs (miRNAs) are approximately 22 nucleotide non-coding RNAs that play a major role in post-transcriptional gene regulation. The seed region of miRNAs bind to the 3'-untranslated regions (UTRs) of target mRNA and facilitate either mRNA degradation or translational repression by limiting ribosomal mobility (Guo et al., 2010; Lewis et al., 2005). A single miRNA can regulate hundreds of genes, meaning that altering the expression of one miRNA can modulate entire gene programs (Lewis et al., 2005; Lewis et al., 2003). MiRNA manipulations promote axon outgrowth in cell lines (Nampoothiri and Rajanikant, 2019; Su et al., 2020; van Battum et al., 2018; Wang et al., 2020; White and Giffard, 2012; Zhang et al., 2011) primary cortical neurons (Hintermayer et al., 2024; Liu et al., 2013; Lu et al., 2015; Qin et al., 2023; Wang et al., 2023; Zhang et al., 2020a, 2020b), primary retinal neurons (Han et al., 2015; Hintermayer et al., 2024; Mak et al., 2020), and dissociated DRGs (e.g. Hancock et al., 2014; Strickland et al., 2011; Wang et al., 2019; Zhao et al., 2021). *In vivo*, miRNA modulations in neurons promote axon regeneration in the rodent optic nerve (Cong et al., 2024; Hintermayer et al., 2024; Lukomska et al., 2024; Mak et al., 2020; van Battum et al., 2018), sciatic nerve (Cong et al., 2024; Zhang et al., 2020a, 2020b; Zhao et al., 2021), and spinal cord (Dai et al., 2018; Gaudet et al., 2016). MiRNAs may also be necessary for endogenous axon regeneration, as the impairment of miRNA biogenesis via DICER knockout diminishes conditioning lesion-induced regeneration (Wu et al., 2012).

Sustained miRNA inhibition is challenging due to the rapid degradation of linear RNA inhibitors. Locked nucleic acid (LNA) inhibitors resist degradation but cannot be directed to specific cell types (Rasmussen and Roberts, 2007). MiRNA gene deletion offers stable knockout but risks disrupting host genes or clustered miRNAs, and fails to account for paralogous loci (Momin et al., 2021). In contrast, endogenous circular RNAs naturally sequester miRNAs (Panda, 2018; Xiao et al., 2022), inspiring the development of engineered circRNA sponges that inhibit miRNAs with high stability due to their exonuclease-resistant closed-loop structure (Lavenniah et al., 2020).

In this study, scRNA seq datasets from mouse DRGs subjected to conditioning lesion were analyzed to identify a core set of RAGs. Using an *in silico* pipeline, we then identified miRNAs potentially regulating these genes and designed a novel circRNA sponge targeting miR-340-5p. We assessed its impact on gene expression, axon regeneration, and RGC survival at both acute and chronic timepoints following ONC. Our findings demonstrate that miRNA-targeting RNA therapeutics are a promising strategy for promoting axonal regeneration and neuronal survival.

2. Methodology

2.1. Literature search

A literature search was performed on PubMed on March 1, 2021 to identify single-cell RNA sequencing (scRNA-seq) datasets from DRG neurons subjected to a conditioning lesion. The following Boolean query was used: (“High-Throughput Nucleotide Sequencing”[Mesh] OR

(“Sequence Analysis, RNA”[Mesh] OR RNA seq)) AND (“Nerve Regeneration”[Mesh] OR Nerve Regeneration). This search retrieved 67 research articles published between 2011 and 2021. Studies were included if they met all the following criteria: (1) scRNA-seq data were available, (2) DRGs were isolated from wild-type mice, and (3) cells were collected 7 days after conditioning lesion. After applying these criteria, two studies were identified for analysis: Renthal et al. (2020) and Hu et al. (2016).

2.2. Neuronal culture, transduction and reseeding

All animal procedures were approved by the Montreal Neurological Institute Animal Care and Use Committee, following the Canadian Council on Animal Care (CCAC) guidelines. Mouse and rat cortical neuron cultures were prepared as previously described (Paré et al., 2018). For reseeding assays, cortical neurons from E18 Sprague-Dawley rat pups were cultured on 96-well plates coated with poly-L-lysine (PLL) at 30,000 cells/well in NeuroBasal (Gibco) supplemented with 1 % Glutamine, 2 % B27, and 1 % N2. For transduction experiments, neurons were infected with lentivirus at a multiplicity of infection (MOI) of 1.0 at 1DIV for 24 h. For adeno-associated virus serotype 2 (AAV2) transduction experiments, high titer AAV2 (genome copies $\sim 10^{12}$) were added to neurons at 1DIV at 1:1000 titer with supplemented NeuroBasal for 24 h. For reseeding experiments, neurons were digested with 0.25 % Trypsin-EDTA for 10 min at 37 °C, 5 % CO₂ to retract all neuronal processes, followed by replating on fresh PLL-coated 96-well plates in DMEM with 10 % FBS and Pen/Strep at 10,000 cells/well. After one hour, media was replaced with supplemented NeuroBasal. For retinal neuron cultures, E16 Sprague-Dawley rat retinas were digested with papain (Worthington) for 30 min at 37 °C and 5 % CO₂ as per manufacturer’s instruction. Cells were triturated and then pelleted by centrifugation at 300 RCF for 5 min at RT. The supernatant was removed, and the cell pellet was resuspended with 1 mL DMEM with 10 % FBS and Pen/Strep. Cells were plated onto 96-well plates coated with PLL (0.1 mg/mL) and Laminin (4 µg/mL) and cultured in supplemented NeuroBasal. Retinal neurons were transfected at 2DIV with miRCURY LNA miRNA inhibitors or mimics (Qiagen) at a final concentration of 20 nM using Hiperfect transfection reagent (Qiagen) as per manufacturer’s instruction. For all neuronal culture experiments, half of the media volume was replaced with fresh supplemented NeuroBasal every 2–3 days until the experimental endpoint.

2.3. Immunocytochemistry and *in vitro* microscopy

Neurons were fixed with 4 % paraformaldehyde (PFA), permeabilized with 0.5 % Triton-X and blocked with 5 % bovine serum albumin (BSA) fraction V prior to primary antibody incubation. Neurons were stained with β-III-Tubulin antibody (1:1000 Rabbit αTUJ1, ThermoFisher) in 1 % BSA overnight at 4 °C, followed by incubation with fluorescently conjugated secondary antibodies (1:1000 Goat αRabbit AlexaFluor-568, ThermoFisher) and DAPI nuclear stain for two hours at RT. Images were acquired using an ImageXpressMicro high-content screening microscope (Molecular Devices), and neurite outgrowth for GFP-TUJ1 double-positive neurons was quantified using the MetaXpress Neuronal Process analysis module. Two complementary outcome measures were assessed to quantify neurite outgrowth: mean neurite outgrowth and maximum neurite outgrowth. For mean cortical neuron outgrowth, the neurite length of every cell was measured and a single mean value from 2 to 3 technical replicates was calculated for each biological replicate. For the maximum neurite outgrowth metric, the three longest neurites within each technical replicate were identified and their lengths averaged. This analysis yielded 2–3 data points per biological replicate, which are reported. For retinal neurons, mean neurite outgrowth per cell was measured, and data from six individual technical replicates across three separate biological replicates were reported.

2.4. Virus production

Lentivectors encoding antagonmir miRNA inhibitors (*i.e.* miR-OFF) were purchased from Applied Biological Materials (ABM) and transfected into HEK293T cells along with helper plasmids (pRSVREV, pMD2G, pMDLG/pRRE) using Lipofectamine-2000 (Invitrogen) transfection reagent as per manufacturer's instruction. Viruses were collected at 48- and 72-h post-transfection, and isolated as previously described (Tang et al., 2015). The functional titer of concentrated virus was determined in HEK293T cells by determining the percentage of GFP-positive cells following 24-h virus incubation, as previously described (Labisch et al., 2021). Custom AAV2 virus was produced by the Viral Core at Boston Children's Hospital.

2.5. RNaseR digestion and sponge circularization confirmation

Plasmid DNA encoding Circ-340-5p was transfected into HEK293T cells at 50 % confluence using Lipofectamine-2000 (Invitrogen) transfection reagent according to manufacturer's instruction. RNA was extracted using the RNeasy mini preparation kit (Qiagen) as per manufacturer's instructions. For RNaseR digestion, 2 µg of total RNA was digested with RNaseR (ThermoFisher) at 37 °C, followed by RNA purification using the RNeasy mini preparation kit. cDNA synthesis was conducted using the iScribe reverse transcriptase kit (BioRad) as per manufacturer's instructions. Convergent (forward: 5'-GTAAAGGTACG-TACTAATGAC-3'; reverse: 5'-CCTCGCGCGTTAACGAGCTCC-3'), divergent (forward/pre: 5'-GTCATTAGTACGTACCTTTAC-3'; reverse/post 5'-GCAGCTCGTTAACCGCGGGAGG-3'), or *Gfp* (forward: 5'-GCTTCCCCG TATGGCTTCATTTCTCC-3'; reverse: 5'-CTAGTTGTGGTTGTCCAA ACTCATCAATG-3') primers were utilized to amplify total and circularized Circ-340-5p cDNA product or *Gfp*, respectively. RT-PCR product was run on a 1 % agarose gel with ethidium bromide and visualized using an ImageDoc (BioRad) scanner.

2.6. Luciferase assays

HEK293T cells were seeded into black-walled 96-well plates and co-transfected with miRCURY LNA miRNA mimics for mmu-miR-340-5p or a non-targeting control (Qiagen) at 20 nM and 3'UTR dual luciferase constructs (GeneCopoeia) at 200 ng/well using Lipofectamine-2000 (ThermoFisher) as per manufacturer's instruction. Luminance was determined 24 h following transfection with the Luc-Pair Duo-Luciferase HS assay kit (GeneCopoeia) using an Enspire microplate reader (PerkinElmer). For the assessment of miRNA sponging, HEK293T cells were transfected with DNA plasmids encoding Circ-340-5p or Circ-Ctrl (200 ng/well) 48 h prior to miRNA/3'UTR co-transfection. Measures of firefly luciferase activity were normalized to renilla luciferase activity for each well.

2.7. In vivo intravitreal injection and optic nerve crush (ONC)

For all animal studies, equal numbers of male and female mice were utilized. For virus delivery, the left vitreous chamber of the eyes of C57BL/6 mice (2–3 months old) were injected with 2 µL of AAV2 encoding Circ-Ctrl or Circ-340-5p using a custom-made glass micro-needle (Wiretrol II capillary, Drummond Scientific Co) as conducted previously (Hintermayer et al., 2024). Under isoflurane anesthesia, micro-scissors were used to expose the sclera, and the microneedle was used to inject into the vitreous chamber at a 45° angle behind the limbus to avoid any injury to the lens. The full volume was slowly injected, and the needle was held in place for 30 s to ensure mixture of the virus with the vitreous.

Two weeks following intravitreal AAV2 injection, ONC was conducted as done previously (Hintermayer et al., 2024). Under anesthesia, the left optic nerve was exposed and crushed 0.5–1.0 mm behind the eye using super fine No. 5 forceps (FSI), applying light pressure for 10 s.

Following ONC, retinal perfusion was confirmed to verify the vascular integrity of the eye. The right optic nerves were not crushed and served as control tissue.

Two days prior to euthanasia, 2 µL of Alexa 647-conjugated cholera toxin beta (Ctβ; Invitrogen) at 5 µg/µL was intravitreally injected into the left eyes of mice to allow for the visualization of regenerating axons in the optic nerve. Intravitreal injections were conducted using the same protocol as for the AAV2 injections above using the same entry point as before to prevent the creation of two holes in the eye.

2.8. Tissue processing and immunohistochemistry

At endpoint, animals were transcardially perfused with ice-cold PBS, followed by 4 % PFA. Eyes and optic nerves were dissected and placed in 4 % PFA overnight at 4 °C. Nerves were transferred to 30 % sucrose/PBS and incubated at 4 °C. Retinas for cross-section were anteriorly dissected into eye cups and were placed in 30 % sucrose/PBS to cryoprotect at 4 °C. Once tissue had sunk in 30 % sucrose/PBS, nerves and eye cups were embedded in Tissue-Tek® optimal cutting temperature (OCT) blocks and cryosectioned at 12 µm. Nerve sections were imaged using an LSM-900 confocal microscope with a 20× objective using tiling. Two-to-four non-consecutive optic nerve sections were quantified for the number of Ctβ fibers at 250 µm intervals from the crush site by blinded raters. The number of axons at each distance was estimated as per Leon and colleagues (Leon et al., 2000). Retinal sections were blocked with 5 % BSA in 0.5 % Triton-X at RT for one hour followed by overnight incubation at 4 °C with primary antibody against ABCA1 (1:250; Abcam; ab18180), AZIN1 (1:500; Sigma; WH0051582M1), CTTN (1:250; Abcam; ab81208), ITGB1 (1:250; Sigma; MAB2079Z), KLF6 (1:200; Sigma; HPA069585), MMP16 (1:500; Invitrogen; 701,306), MYO10 (1:250; Atlas; AMAb91554), NDST1 (1:250; ProteinTech; 26,203-1-AP), RHOC (1:500; Abcam; ab180785), pS6 (1:500; Cell Signalling; 2211), SOX11 (1:100; Millipore; MABE1935), TMEM43 (1:200; Abcam; ab184164), TRKB (1:25-; 80E3 Cell Signalling; 4603), pTRKB (1:250; Sigma; ABN1381), or ZFP664 (1:100; Sigma; SAB2106936). Fluorescently conjugated secondary antibodies (1:500) were incubated in blocking solution for two hours at RT prior to mounting coverslips with Fluoromount G (ThermoFisher). Retinal cross-sections were imaged using a 20× objective on an LSM-900 confocal microscope. Fluorescence quantification was conducted by raters blinded to the experimental condition using ImageJ software.

For retinal wholemounts, fixed eyes were anteriorly dissected, and retinas were gently removed from the eye cups using paint brushes. Four radial cuts were made to form the retina into a cloverleaf. Retinas were washed three times with 0.5 % Triton-X in PBS at RT, followed by freezing in 0.5 % Triton-X/PBS at –80 °C for 15 min to permeabilize tissue. Retinas were washed again and blocked overnight in 5 % BSA in 0.5 % Triton-X at 4 °C. The following day, primary antibody against BRN3A (1:500; Millipore; MAB1585) was added to blocking solution and incubated at 4 °C for three days. Retinas were washed and incubated overnight at 4 °C with fluorescently conjugated secondary antibody (1:500) and DAPI nuclear stain in blocking solution. The next day, retinas were washed and cover slipped. Wholemount retinas were imaged using an LSM-900 confocal microscope with a 20× objective, and a sample of 4–6 images taken at three distances from the optic disc were taken for quantification of BRN3A-positive cells. DAPI and BRN3A double-positive cells were quantified by a blinded observer for each image. The number of DAPI-BRN3A double-positive cells was normalized to the uninjured contralateral eye to establish the percentage of surviving BRN3A-positive RGCs in each mouse.

2.9. Statistical analyses

Experimental design, biological replicates, and statistical analyses are indicated in figure legends, including: two-tailed student's *t*-test, one-way analysis of variance (ANOVA), two-way ANOVA, and *post-hoc*

Šídák's multiple comparisons tests. All statistical analyses were conducted using GraphPad Prism 6. Normality of data was assessed for all comparisons, and non-parametric tests used when normality was violated. Statistical significance was defined as $*p < .05$, $**p < .01$, $***p < .001$, $****p < .0001$.

3. Results

3.1. In silico prediction of regeneration-associated miRNAs from scRNA sequencing datasets

Existing sequencing datasets from the DRG conditioning lesion paradigm were used to predict miRNAs that may regulate multiple genes implicated in the regeneration program. A systematic literature search was conducted to identify scRNA-seq datasets from wild-type mouse DRGs following conditioning lesion paradigm. Our search identified two high-quality mouse scRNA-seq datasets from regenerating DRGs which were analyzed to characterize conserved transcriptional changes within regenerating DRG neurons (Hu et al., 2016; Renthal et al., 2020). A shared pool of 104 RAGs were differentially expressed in both datasets seven days following conditioning lesion (Fig. 1A). The seven-day timepoint was chosen because it corresponds to the peak of growth-associated protein 43 expression in this model (GAP-43; Dubový et al., 2019). Additionally, DRG explants harvested seven days after conditioning lesion show a robust regenerative phenotype in culture, indicating that RAG programs are active at this time (Dubový et al., 2019; Niemi et al., 2022). Fold changes in RAG expression levels were highly correlated between these two scRNA-seq datasets, showing a consistent direction of regulation for each gene ($r^2 = 0.81$, $p < .0001$; Fig. 1A). Statistical enrichment analysis of these RAGs highlighted biological processes and KEGG pathway terms implicated in axon regeneration, including cell projection organization, PI3K/mTOR signalling, and nervous system development (Fig. 1B).

A miRNAome-wide bioinformatics approach was applied to analyze all 1983 mouse miRNAs annotated on miRBase (Kozomara et al., 2019) and identify those predicted to simultaneously target multiple RAGs by pairing with their 3'UTRs (Fig. 1C). The miRGate database was used to generate miRNA target predictions, as it incorporates computational algorithms from microtar, RNAHybrid, miRanda, TargetScan, and Pita, applied to a common reference mouse genome (Andrés-León et al., 2015). Individual miRNAs had predicted interactions with between 1 and 55 RAGs (Fig. 1D). To select miRNAs that were most likely to target RAGs, this list was then filtered to include only those miRNAs having at least one experimentally validated interaction with at least one RAG, as determined by inclusion in the miRTarBase database (Chou et al., 2016; Huang et al., 2022). From this list, eight miRNAs (miR-124-3p, miR-15a-5p, miR-17-5p, miR-181a-5p, miR-24-3p, miR-340-5p, miR-758-3p, and miR-9-5p) were prioritized based on the total number of miRNA-RAG interactions predicted. A STRINGdb protein-protein interaction network (Szklarczyk et al., 2023) depicts the large degree to which core RAGs are predicted to be targeted by the top eight miRNA candidates (Fig. 1E; Supplemental File 1). Thus, an analysis of existing scRNA seq datasets from the literature defines a conserved gene program consisting of 104 RAGs, that are largely targeted by eight key miRNAs.

3.2. The inhibition of miR-340-5p promotes neurite outgrowth in multiple cell types *in vitro*

Since miRNAs generally suppress the expression of their target genes, we postulated that inhibitors targeting these miRNAs would derepress RAGs and promote regeneration. To test this hypothesis, the effects of miRNA inhibitors were screened *in vitro* by assessing their impact on the outgrowth of dissociated cortical neurons. A miRNA expression atlas confirmed that the eight prioritized miRNAs were expressed in mouse neocortex (Fig. 2A; He et al., 2012; Hoye et al., 2017). Embryonic cortical neurons were transduced with lentiviruses encoding antisense

miRNA inhibitors for 72 h. Neurons were then trypsinized and reseeded to remove all processes and restart neurite growth (Fig. 2B). Following reseeding no significant changes in baseline cell survival were noted between miRNA inhibitor groups (Supplemental Fig. 1). Inhibitors targeting four miRNAs (miR-340-5p, miR-24-3p, miR-17-5p, and miR-758-3p) significantly increased mean neurite outgrowth per cell (Fig. 2C, D). To identify miRNA inhibitors that may favor long distance neurite extension rather than extensive neuritogenesis and short distance growth, the length of the three longest neurites in GFP-positive neurons was averaged for each technical replicate. In this analysis, miR-340-5p inhibition produced the longest growth profile (Fig. 2E). Genetic modulations that target core regenerative programs are likely to promote regeneration in multiple types of CNS neurons (e.g. Otake et al., 2015). To determine whether the outgrowth effect of miR-340-5p inhibition is conserved between multiple neuronal subtypes, neurite outgrowth was also assessed in rat embryonic retinal neurons transfected with an LNA miRNA inhibitor (LNA-340-5p; Fig. 2F). Reseeding was not performed in these experiments, as transfected retinal neurons are more sensitive to this stress than cortical neurons in culture and do not reliably survive reseeding. Consistent with the findings in cortical neurons, miR-340-5p inhibition increased mean neurite outgrowth in retinal neurons (Fig. 2G, H). These results demonstrate that miR-340-5p inhibition promotes neurite outgrowth *in vitro* in multiple neuronal types and support its prioritization as a strategy to target multiple RAGs to enhance axon regeneration.

3.3. MiR-340-5p targets numerous RAGs, and members of regeneration signalling pathways

Since miRNAs often target groups of functionally related genes, miR-340-5p inhibition may contribute to neurite outgrowth by simultaneously regulating RAGs along with other key genes in related pathways. To describe the effects of miR-340-5p on gene expression, we compiled a list of target genes using the miRTarBase database of experimentally validated miRNA interactions and the CLEAR-CLIP dataset from Moore et al., which contains *in vivo* mouse brain miRNA-target interactions (Chou et al., 2016; Huang et al., 2022; Moore et al., 2015). Since miR-340-5p inhibition produces outgrowth phenotypes in both cortical and retinal neurons, target genes were filtered to include those expressed in both cortical neurons *in vitro* and fluorescence-activated cell sorted retinal ganglion cells (RGCs; Fig. 3A). Pathway analysis was conducted using STRINGdb (Szklarczyk et al., 2023), revealing numerous overrepresented pathways involved in regeneration and survival, including axon guidance, PI3K signalling, neurotrophin signalling, and MAPK signalling, among others (Fig. 3B). Therefore, miR-340-5p is predicted to target numerous genes in key pathways in addition to RAGs that are expressed in conditioned DRG neurons.

To experimentally confirm that miR-340-5p regulates members of this RAG program, luciferase assays were performed to assess its effects on a subset of RAGs. A prioritized list of key miR-340-5p targets was generated based on their inclusion in the miRTarBase database of experimentally validated miRNA targets and their prediction by at least two computational algorithms, including: *Myo10*, *Ndst1*, *Azin1*, and *Abca1*. *Ctnn* was added to include a target with a less stringent prediction threshold (Fig. 3C). Dual luciferase assays were conducted by cotransfected HEK293T cells with luciferase constructs encoding the luciferase gene flanked by the full 3'UTR sequence of RAGs (Fig. 3D). These assays demonstrated that miR-340-5p targets the 3'UTR and regulates the expression of *Myo10*, *Ndst1*, *Azin1*, and *Abca1*, but not *Ctnn* (Fig. 3E). Thus, miR-340-5p regulates the expression of numerous RAGs *in vitro* as predicted by our *in silico* analysis.

3.4. The generation of a circularized miR-340-5p sponge

A potent and sustainable inhibitor against miR-340-5p was

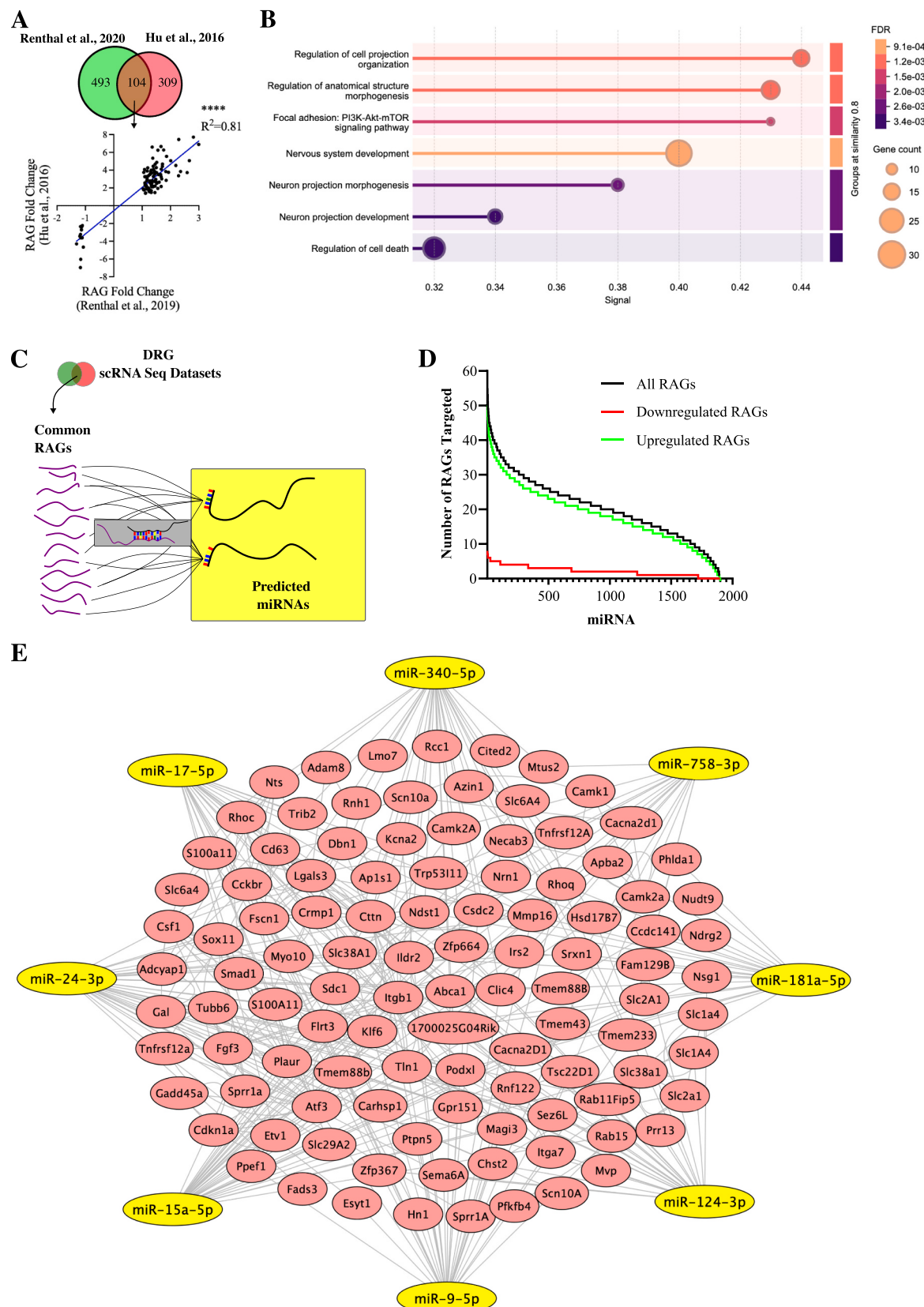


Fig. 1. In silico prediction of RAG-targeting miRNAs. (A) Overlap of RAGs in DRGs seven days following conditioning lesion (Renthal et al., 2020; Hu et al., 2016). Individual datapoints represent individual RAGs. Solid line represents linear regression. (B) Statistically enriched biological processes and KEGG pathways for RAGs. (C) Schematic representation of *in silico* approach for identifying regeneration-associated miRNAs. (D) Plot displaying the number of RAGs targeted by each miRNA, ranked by the total number of targets. (E) STRING network of protein-protein interactions between RAGs (red), and candidate miRNAs targeting RAGs (yellow). **** $p < .0001$. (For interpretation of the references to colour in this figure legend, the reader is referred to the web version of this article.)

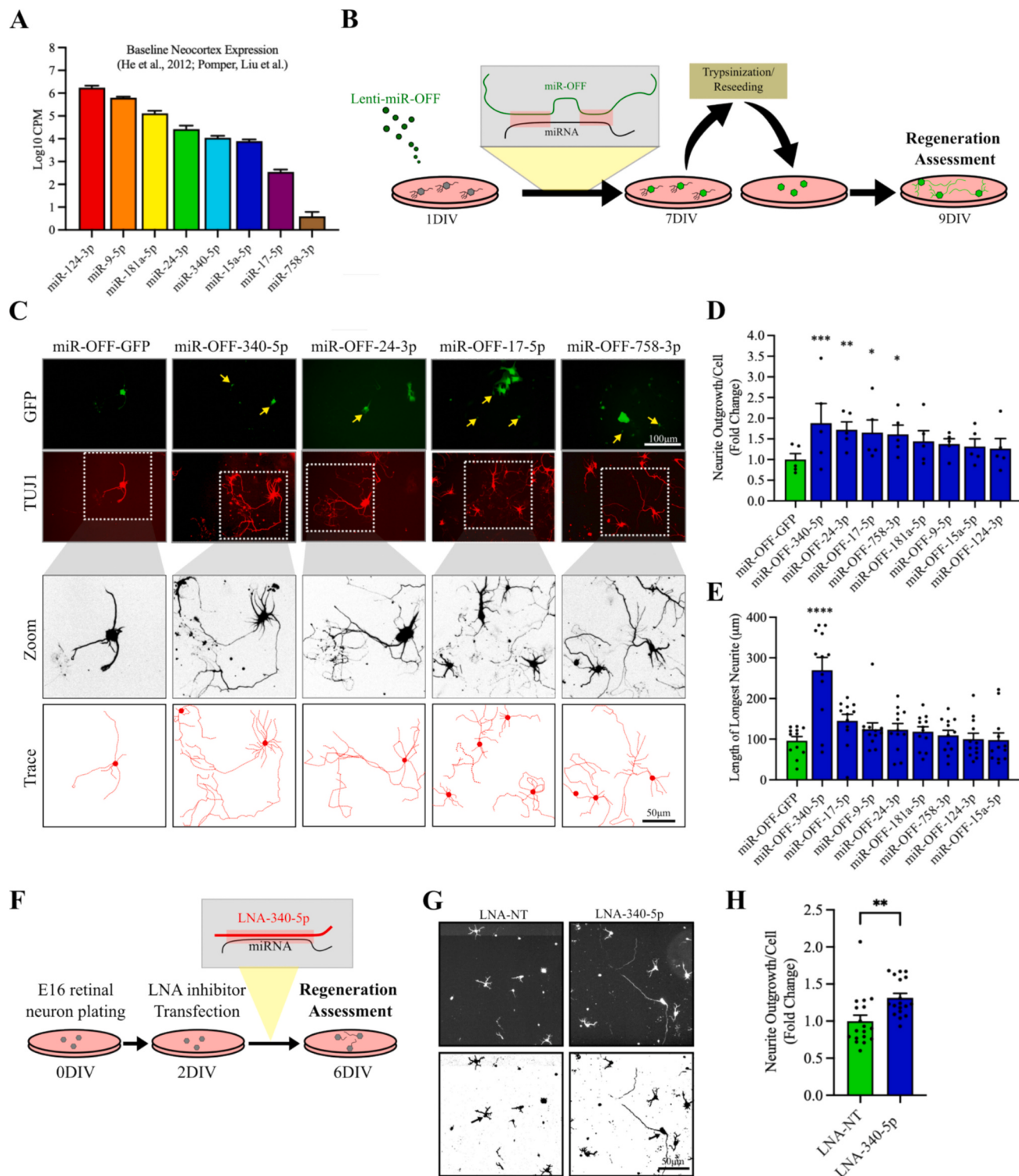


Fig. 2. MiR-340-5p inhibition promotes neurite regeneration in multiple neuronal cell types in vitro. (A) miRNA expression in bulk mouse neocortex, based on expression datasets from He and colleagues, and Pomper Liu and colleagues (He et al., 2012; Pomper et al., 2020). (B) Experimental paradigm for reseeding experiments. Neurons were transduced with lentivirus miRNA inhibitors at 1DIV and trypsinized and reseeded at 7DIV. Cells were fixed at 9DIV and stained with antibodies against βIII-Tubulin (TUJ1) for high-content screening analysis of neurite regeneration. (C) Representative images of cortical neurons stained with antibody against TUJ1 to visualize processes. Arrows indicate GFP-TUJ1 double-positive neurons (scale bar = 50 μm). (D) Quantification of mean neurite outgrowth per cell, where each data point represents the mean value from a single biological replicate ($n = 4\text{--}5$, one-way ANOVA, Sídák's multiple comparisons test). (E) Quantification of the average of the three longest neurites per well, shown as individual technical-replicate data points (2–3 wells per biological replicate; $n = 4\text{--}5$ biological replicates per condition; one-way ANOVA with Sídák's multiple comparisons test). (F) Schematic of retinal neuron outgrowth experiment. (G) Representative image of embryonic retinal neurons transfected with non-targeting LNA (LNA-NT) or an LNA against miR-340-5p (LNA-340-5p) stained with antibodies against TUJ1 (scale bar = 50 μm). (H) Quantification of mean neurite length per cell, where each data point represents an individual technical replicate (six wells across three biological replicates; unpaired *t*-test). Error bars represent standard errors of the mean (SEM). * $p < .05$, ** $p < .01$, *** $p < .001$, **** $p < .0001$.

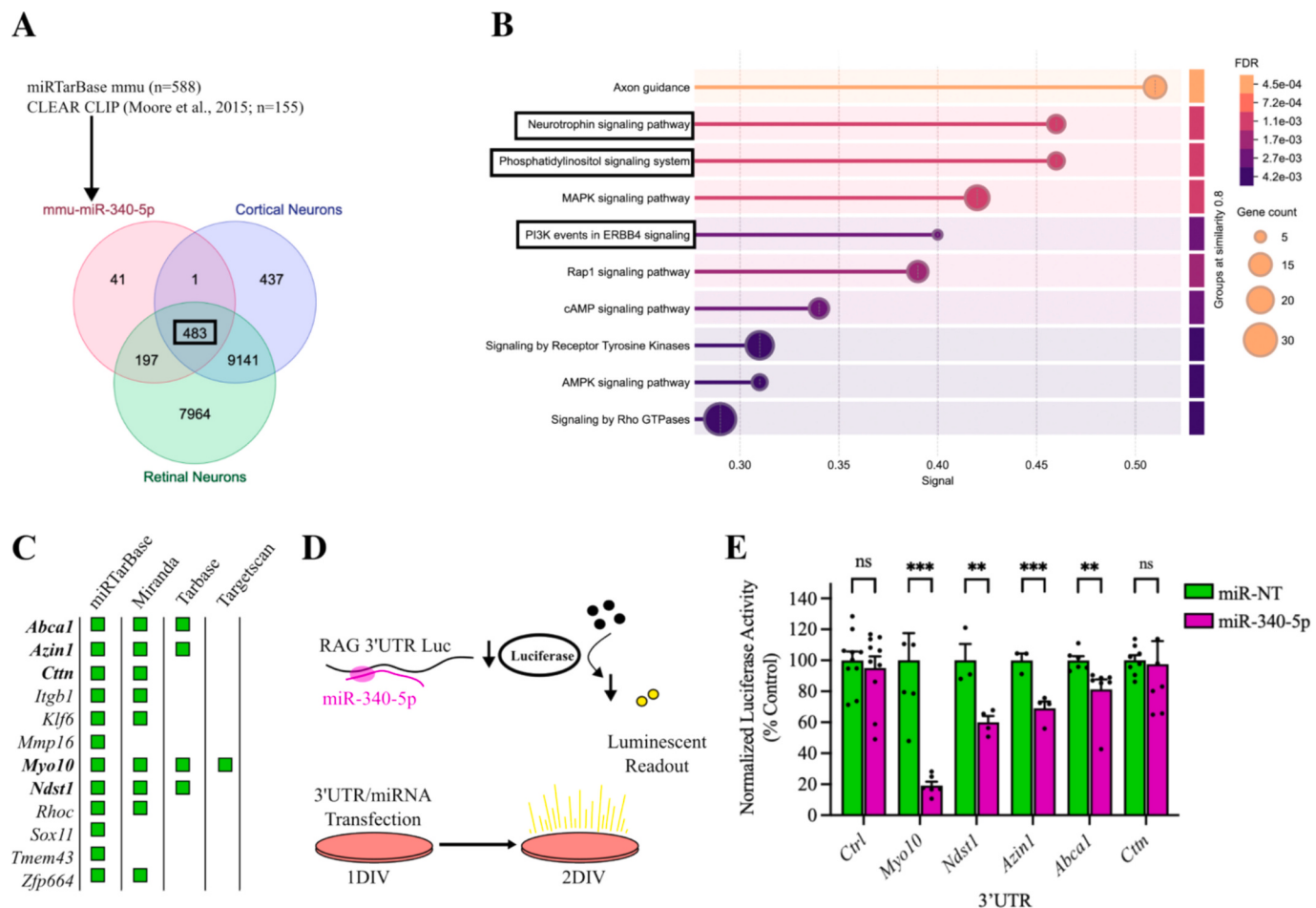


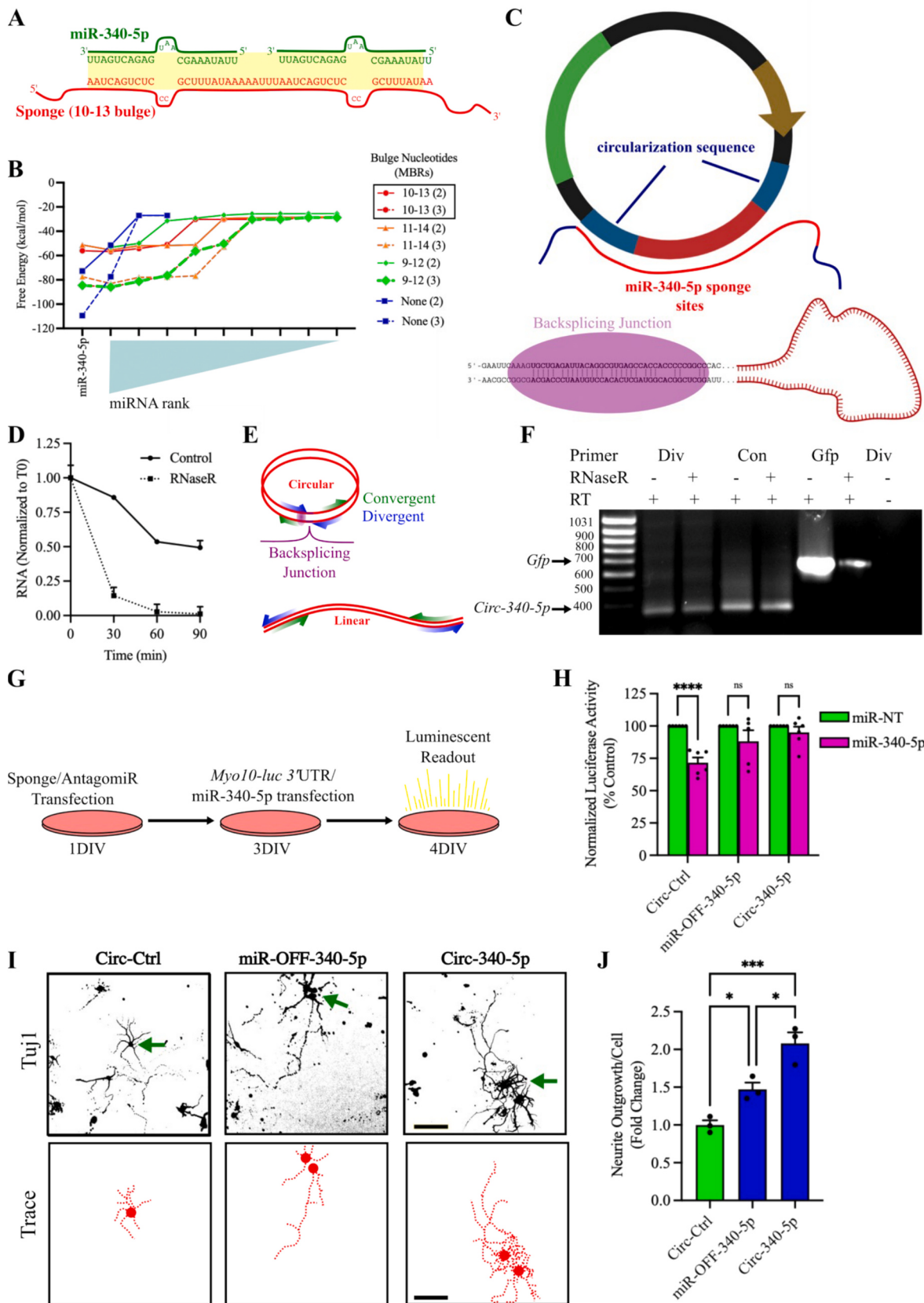
Fig. 3. miR-340-5p targets numerous RAGs and regulates regeneration pathways. (A) Compilation of miR-340-5p target gene list for pathway analysis, including those from the miRTarBase database and the CLEAR-CLIP *in vivo* mouse brain dataset (Chou et al., 2016; Huang et al., 2022; Moore et al., 2015). (B) Statistically enriched Reactome and KEGG pathways for broad list of miR-340-5p targets. (C) Assessment of the number of *in silico* computational algorithms predicting miR-340-5p targeting subset of RAGs from the miRTarBase validated database. Bolded genes are those selected for *in vitro* luciferase assay. (D) Schematic of luciferase assay experimental design. (E) Luciferase assays for selected RAGs (n = 4–10/condition, unpaired t-test). Error bars represent standard errors of the mean (SEM). *p < .05, **p < .01, ***p < .001, ****p < .0001.

developed for *in vivo* regeneration studies. While antisense RNAs containing a single miRNA binding site can be expressed in cells to inhibit miRNAs, their effects are diminished by exonuclease-mediated RNA transcript degradation and canonical miRNA-mediated target RNA decay (Meister et al., 2004; Nishihara et al., 2013). MiRNA sponges encode complementary decoy RNA sequences that can be packaged into DNA viruses for transduction and expression in specific cell types. MiRNA sponges are potent miRNA inhibitors because they contain multiple miRNA binding sites (MBS) per transcript. Further, the stability of miRNA sponges can be improved through circularizing the RNA. Circular RNAs (circRNAs) endogenously function as miRNA sponges and, lacking 3' or 5' ends, are resistant to many RNA degradative processes in cells, increasing their longevity and potentially their efficacy (Ebbesen et al., 2016; Panda, 2018; Xiao et al., 2022; Zhou et al., 2020). CircRNAs can be constitutively expressed in cells and mediate long-term sequestration and functional inhibition of miRNAs (Lavenniah et al., 2020; Zhu et al., 2024).

A circularized miR-340-5p sponge (Circ-340-5p) was developed for the purpose of achieving potent and sustained miR-340-5p inhibition *in vivo*. A sponge sequence targeting miR-340-5p and a scrambled control sponge sequence were generated using the miRNAsong *in silico* algorithm (Fig. 4A; Barta et al., 2016). Sponge sequences with 10–13 nt bulges were generated to reduce interference-like RNA cleavage and rapid sponge degradation observed with those possessing perfect

antisense complementarity to miRNAs (Ebert et al., 2007; Kluiver et al., 2012b; Kluiver et al., 2012a). The specificity of these sponges was assessed *in silico* by examining the free energy of association between the chosen sponge sequence and all other murine miRNAs. This analysis revealed that our sponge had a high affinity for miR-340-5p with minimal off-target effects on other miRNAs (Fig. 4B). To promote circularization, sponge sequences were inserted between flanking complementary intronic binding sequences (*i.e.* ‘circularization sequences’) from the *circHIPK3* gene. This strategy has previously been employed to enhance the circularization of various RNA sequences (Liang and Wilusz, 2014). Six repeats of our miR-340-5p sponge sequence were cloned within these complementary intronic sequences (Fig. 4C).

To confirm that this sponge was forming circularized RNA in cells, we exploited the fact that circRNAs lack 3' and 5' ends and are resistant to RNaseR-mediated degradation (Kristensen et al., 2019; Zhou et al., 2020). An RNaseR digestion protocol was developed to degrade linear RNA species in lysates generated from HEK293T cells (Fig. 4D). Circ-340-5p was expressed in HEK293T cells and RNA lysates were subjected to a 90-min RNaseR digestion to degrade linear RNA species. RT-PCR was conducted using divergent (directed toward the anticipated back splicing site) and convergent (directed toward the center of the sponge) PCR primers to amplify circularized and total Circ-340-5p sponge, respectively (Fig. 4E). The presence of our sponge as a PCR



(caption on next page)

Fig. 4. The design and generation of a circularized sponge targeting miR-340-5p. (A) Complementary binding of miR-340-5p with two repeating sequences of Circ-340-5p separated by a 6 nt spacer sequence. (B) *In silico* assessment of free energy of association between Circ-340-5p to miR-340-5p when compared with all other miRNAs in the mmu genome. MiRNAs are ranked with respect to their free energy of association. (C) Schematic of Circ-340-5p plasmid organization and sponge synthesis *in vitro*. Circularization sequences adapted from Liang and Wilusz (2014). (D) Quantification of RNA concentration in lysates containing Circ-340-5p in response to RNaseR digestion ($n = 2$). (E) Schematic demonstrating concept of divergent and convergent primers with respect to circular RNA PCR product amplification. Convergent (standard) primers point toward the center of linear RNA transcripts, whereas divergent primers point toward the predicted back splicing junction of circular RNAs. (F) Products of PCR amplification run on agarose gel. (G) Schematic of luciferase assay to test Circ-340-5p sponging effectiveness. (H) Luciferase assay for miRNA sponge inhibitors using luciferase flanked by the 3'UTR of Myo10 ($n = 6$; two-way ANOVA, Šídák's multiple comparisons test). (I) Representative images and trace of neurite regeneration with miRNA inhibitors (scale bar = 50 μ m). (J) Quantification of neurite regeneration as mean neurite outgrowth per cell ($n = 3$; one-way ANOVA, Šídák's multiple comparisons test). Error bars represent standard errors of the mean (SEM). * $p < .05$, ** $p < .01$, *** $p < .001$, **** $p < .0001$.

product amplified by divergent primers, and the maintenance of this PCR product following 90-min RNaseR treatment is consistent with a degradation-resistant circularized RNA (Fig. 4F).

The efficacy of Circ-340-5p in sequestering miR-340-5p was tested by luciferase reporter assay using a *Myo10-3'UTR-luc* construct. HEK293T cells were transfected with plasmids encoding Circ-Ctrl, Circ-340-5p, or linear miR-OFF-340-5p. Two days later, a luciferase construct for *Myo10-3'UTR-luc* was co-transfected with a miR-340-5p mimic or a non-targeting miRNA control, and luminescence was read after 24 h (Fig. 4G). This assay revealed that linear miR-OFF-340-5p diminished the effects of miR-340-5p on reducing *Myo10-3'UTR-luc* expression. Circ-340-5p virtually eliminated the effect of miR-340-5p on *Myo10-3'UTR-luc* expression, suggesting highly efficient miRNA sequestration (Fig. 4H). Thus, Circ-340-5p effectively sequesters miR-340-5p, preventing a reduction in *Myo10-3'UTR-luc* expression. To confirm that Circ-340-5p exhibited phenotypes consistent with miR-340-5p inhibition in neurons, Circ-Ctrl and Circ-340-5p were packaged into lentiviruses for cortical neuron transduction experiments. Cortical neurons were transduced with lenti-Circ-Ctrl, lenti-miR-OFF-340-5p, or lenti-Circ-340-5p and were subjected to trypsinization and reseeding as conducted previously to assess neurite outgrowth. Consistent with our earlier experiments, miR-OFF-340-5p promoted neurite outgrowth following reseeding (Fig. 4I, J). Circ-340-5p enhanced this effect, leading to a further increase in the mean neurite outgrowth per cell following reseeding (Fig. 4I, J). Thus, Circ-340-5p circularizes in cells, and promotes robust neurite outgrowth *in vitro* when compared to a linear miR-340-5p inhibitor.

3.5. Circ-340-5p de-represses numerous RAGs in retinal ganglion cells

Given that Circ-340-5p effectively sequesters miR-340-5p and promotes neurite outgrowth *in vitro*, the ability of this sponge to disinhibit RAG expression in RGCs *in vivo* was assessed. Circ-340-5p was packaged into AAV2, since this serotype selectively transduces RGCs and some amacrine cells (Auricchio et al., 2001; Pang et al., 2008; Zhang et al., 2019). The *in vivo* assessment of the effects of AAV2-Circ-340-5p on protein expression was focused on RAGs with experimentally validated interactions with miR-340-5p from the miRTarBase database, including: ABCA1, AZIN1, CTTN, ITGB1, KLF6, NDST1, RHOC, ZFP664, MMP16, SOX11, and TMEM43 (Chou et al., 2016; Huang et al., 2022). Intravitreal injections of AAV2-Circ-Ctrl or AAV2-Circ-340-5p were conducted and retinas were harvested two weeks later. Retinal cross-sections were stained with antibodies against RAGs to assess their levels in GFP-positive RGCs. Of the RAGs assessed, Circ-340-5p significantly elevated AZIN1, NDST1, MYO10, and ABCA1, whereas the levels of CTTN, ITGB1, KLF6, RHOC, MMP16, and SOX11 were not significantly altered (Fig. 5A-C). Reliable staining for ZFP664 or TMEM43 could not be achieved.

Since miR-340-5p is predicted to target not only RAGs but also key components of PI3K and neurotrophin signalling (Fig. 3B), members of these pathways were also assessed using immunofluorescence. Because S6 ribosome phosphorylation is a downstream effect of PI3K signalling, pS6 staining was used as a marker of pathway activation (Hay and Sonenberg, 2004; Kanaizumi et al., 2018; Park et al., 2008). Circ-340-5p

elevated the levels of pS6 in RGCs indicating activation of PI3K signalling (Fig. 5D, E). Within the neurotrophin signalling pathway, Circ-340-5p was predicted to target *Ntrk2*, the gene encoding the BDNF receptor, TRKB. While facilitating TRKB/BDNF signalling in RGCs is not associated with optic nerve regeneration, interventions activating this pathway are strongly supportive of post-axotomy survival (Chen and Weber, 2001; Cheng et al., 2002). We reasoned that in addition to promoting axon regeneration via the targeting of RAGs and PI3K signalling, Circ-340-5p might also enhance pro-survival TRKB/BDNF signalling in RGCs. Circ-340-5p elevated the expression of TRKB as well as the level of activated pTRKB in RGCs, indicating the activation of the prosurvival BDNF/TRKB neurotrophin signalling pathway (Fig. 5F-H). Collectively, these data demonstrate that Circ-340-5p simultaneously de-represses multiple RAGs and facilitates the activation of PI3K and TRKB signalling in RGCs.

3.6. Circ-340-5p facilitates the survival of RGCs and promotes optic nerve regeneration following axotomy

Given the finding that AAV2-Circ-340-5p derepressed gene targets for RAGs, PI3K, and TRKB/BDNF signalling, the phenotypic effects of this intervention on both the survival and regeneration of RGCs following ONC axotomy were assessed. ONC was conducted two weeks after intravitreal injection of AAV2-Circ-Ctrl or AAV2-Circ-340-5p, followed by intravitreal injection of fluorescently conjugated cholera toxin beta (Ct β) two days prior to euthanasia to trace regenerating axonal fibers. The survival of RGCs was assessed at both two and six weeks following axotomy by counting the number of BRN3A-positive RGC nuclei in wholemount retinas (Fig. 6A). Two weeks following ONC, RGC survival was significantly improved in retinas treated with Circ-340-5p with 46.9 % of RGCs surviving at two weeks post-ONC compared to 13.6 % in Circ-Ctrl treated retinas. Six weeks following ONC, 3.1 % and 5.4 % of BRN3A-positive cells were remaining in retinas expressing Circ-Ctrl or Circ-340-5p, respectively (Fig. 6B, C). These findings suggest that while Circ-340-5p promotes short-term RGC survival, its protective effect diminishes over time. Axon regeneration was assessed by quantifying Ct β -labeled axons in the optic nerve. In control animals, few axons extended beyond the lesion site. In contrast, Circ-340-5p treatment significantly increased both the number and length of regenerating axons at two and six weeks post-ONC (Fig. 6D, E). Notably, regeneration continued to improve between the two- and six-week timepoints, indicating a sustained pro-regenerative effect of Circ-340-5p (Fig. 6E).

4. Discussion

In the present study, the effects of miRNA modulation on coordinately regulating groups of RAGs to promote axon regeneration and post-axotomy neuronal survival was assessed. An *In silico* analysis of existing scRNA-seq datasets from regenerating DRG neurons was performed to identify core miRNAs potentially involved in their regulation. MiR-340-5p inhibition promoted the growth of neurites in both cortical and retinal neurons *in vitro*. A custom circRNA targeting miR-340-5p (Circ-340-5p) promoted optic nerve regeneration and RGC survival following ONC. Circ-340-5p expression in RGCs simultaneously de-

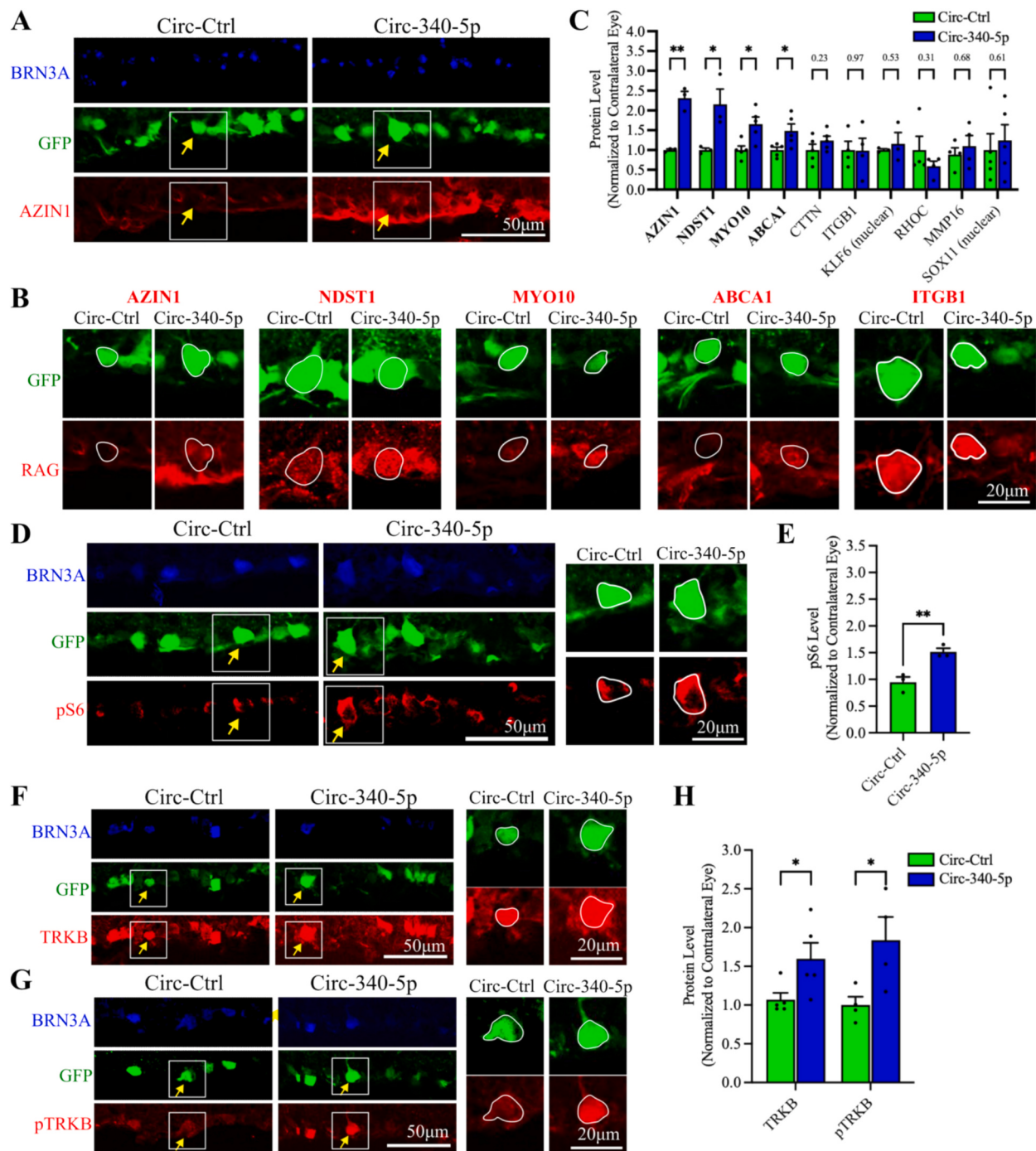


Fig. 5. Circ-340-5p de-represses numerous RAGs in RGCs and regulates PI3K and neurotrophin signalling. **(A)** Representative retinal cross-sections stained for AZIN1 by immunofluorescence. Yellow arrow indicates example of GFP-positive RGC with elevated AZIN1 expression (scale bar = 50 μm). White box demarcates the zoomed-in RGC staining for sample images in panel **B**. **(B)** Representative zoomed-in images of staining for RAGs in GFP-positive RGCs taken from retinal cross sections (scale bar = 20 μm). **(C)** Quantification of RAG protein expression in GFP-positive RGCs. Bolded RAGs were significantly regulated ($n = 3–5/\text{condition}$; unpaired t-test). **(D)** Representative image of pS6 staining in retinal cross-sections (scale bar = 50 μm). Yellow arrow indicates sample RGC, and white box demarcates zoomed-in RGC staining (scale bar = 20 μm). **(E)** Quantification of pS6 staining in RGCs ($n = 3/\text{condition}$; unpaired t-test). **(F, G)** Representative retinal cross section staining for TRKB and pTRKB in RGCs (scale bar = 50 μm). Yellow arrow indicates sample RGC, and white box demarcates zoomed-in RGC staining (scale bar = 20 μm). **(H)** Quantification of TRKB and pTRKB staining in RGCs ($n = 4–5/\text{condition}$; unpaired t-test). Error bars represent standard errors of the mean (SEM). * $p < .05$, ** $p < .01$, *** $p < .001$, **** $p < .0001$. (For interpretation of the references to colour in this figure legend, the reader is referred to the web version of this article.)

repressed multiple RAGs, whilst activating both PI3K and TRKB signalling pathways. Thus, the sustained modulation of a single miRNA can simultaneously disinhibit multiple pro-regenerative and pro-survival signalling pathways in neurons; however, the effects on regeneration of RGCs at later time points is limited by the inability to promote

sustained RGC survival.

Since miRNA sequencing data is not available at single-cell resolution, we leveraged scRNA-seq datasets alongside an *in silico* approach to infer miRNA modulations that mirror gene regulation events in regenerating DRGs. While bulk miRNA seq datasets from DRGs are present in

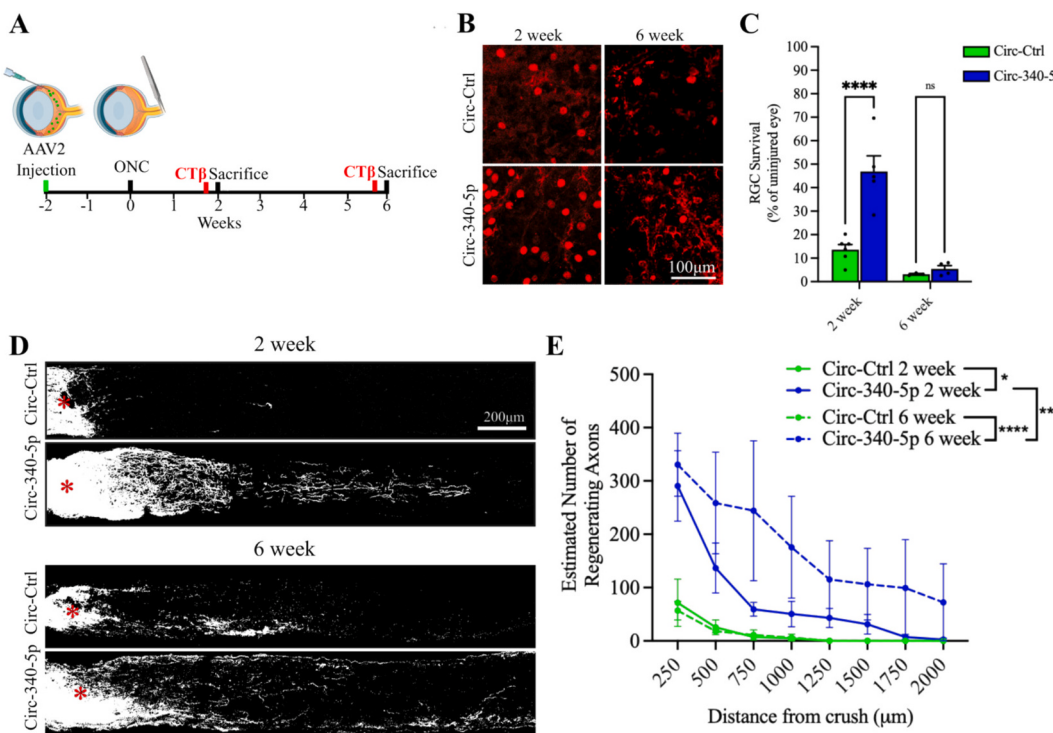


Fig. 6. Circ-340-5p promotes the regeneration and survival of RGCs following axotomy. (A) Schematic of experimental timeline. (B) Surviving RGCs in wholemount retinas at two and six weeks following ONC. RGCs are visualized by BRN3A positivity (scale bar = 100 μ m). (C) Quantification of percentage of surviving RGCs in ipsilateral wholemount retinas compared to the uninjured contralateral retina ($n = 3-5$; unpaired t-test). (D) Optic nerve regeneration with Ct β labeling. Red asterisk denotes the location of ONC (scale bar = 200 μ m). (E) Quantification of estimated regenerating nerves at 250 μ m intervals post-lesion ($n = 3-5$; two-way ANOVA, Šídák's multiple comparisons test). Error bars represent standard errors of the mean (SEM). * $p < .05$, ** $p < .01$, *** $p < .001$, **** $p < .0001$. (For interpretation of the references to colour in this figure legend, the reader is referred to the web version of this article.)

the literature, they reflect the combined miRNA expression data from neurons, glia, and immune cells. Nonetheless, some of the regeneration-associated miRNA changes tested in the present manuscript are also present in bulk miRNA datasets of regenerating DRGs. Notably, two studies of miRNA expression in regenerating DRGs reported downregulation of miR-340, with Yu et al. (2011) additionally identifying reduced levels of miR-124, miR-17, and miR-24 (Phay et al., 2015; Yu et al., 2011). Although non-neuronal cells likely contribute to the observed miRNA downregulation signatures, these findings nonetheless support the notion that DRG regeneration may be regulated by a set of key miRNAs. MiRNA expression changes in RGCs following optic nerve crush have been described (Mead et al., 2021). In that dataset, miR-340-5p was found to be expressed by RGCs, justifying the knockdown approach that we have used to target this miRNA. Expression of miR-340-5p was unchanged in response to injury suggesting that it is not regulated physiologically to impact RGC regeneration.

The simultaneous regulation of multiple RAGs by miR-340-5p was assessed by luciferase reporter assays *in vitro* and via immunofluorescence microscopy in RGCs expressing Circ-340-5p. Immunofluorescence analysis was prioritized over biochemical analysis of proteins since we were specifically interested in protein expression in RGCs, which only comprise ~1 % of the cells in the retina. Of the 12 experimentally validated miR-340-5p target RAGs in the miRTarBase database, four were de-repressed in RGCs by Circ-340-5p: AZIN1, NDST1, MYO10, and ABCA1 (Fig. 5A-C). Given that Circ-340-5p simultaneously de-represses RAGs, it is likely that this construct facilitates regeneration through multiple mechanisms of action, which have been described in the regeneration literature. AZIN1 is an ornithine decarboxylase involved in maintaining polyamine homeostasis in neurons. Ornithine decarboxylation is activated in the facial nerve, in sympathetic nerves, and in DRG neurons during axon regeneration (Gilad and Gilad, 1983; Tetzlaff and Kreutzberg, 1985; Wells, 1987). The elevation in ornithine carboxylase

activity triggered by increased AZIN1 expression could enhance the synthesis of pro-regenerative and pro-survival polyamines, such as spermidine and spermine (Feng et al., 2024; Noro et al., 2015; Olsen and Zetter, 2011). NDST1 is a critical enzyme in heparin sulfate biosynthesis, and the deletion of NDST1 results in altered RGC axonal pathfinding in development, and lens invagination defects (Cai et al., 2014; Missaghian et al., 2022; Pan et al., 2006). Indeed, heparan sulfates are known to be critical in the promotion of axon regeneration, albeit not necessarily *via* neuron-intrinsic mechanisms (Edwards and Hammarlund, 2014; Murakami et al., 2015). MYO10 is increased in regenerating peripheral neurons (Tanabe et al., 2003), and the expression of full length MYO10 is sufficient in promoting neurite outgrowth *in vitro* (Raines et al., 2012). Additionally, MYO10 expression is involved in the trafficking of deleted in colorectal cancer (DCC) to modulate netrin signalling and is required for normal axonal development (Yu et al., 2012; Zhu et al., 2007). ABCA1 is reduced in some patients with open-angle glaucoma, and affects RGC viability by altering cholesterol homeostasis (Yang et al., 2023). Additionally, ABCA1 expression is increased with peripheral nerve injury, and deletion affects the morphology of neurite tips in cortical neurons *in vitro* (Shishioh et al., 2022). Given that each of these RAGs individually contribute to axon regeneration or neuronal viability, it is unlikely that any one of these RAGs are solely responsible for the regeneration observed with Circ-340-5p. A similar concept is seen in oncology research, where miRNAs facilitate multidrug resistance by simultaneously targeting multiple genes within a drug-targeted pathway (Li and Yang, 2013). This fact makes miRNA modulations theoretically more robust activators of regeneration programs in neurons when compared to individual gene modulations owing to their multiple mechanisms of action.

While miRNAs simultaneously target multiple genes within key pathways, an important limitation is that miRNA modulations might simultaneously target positive and negative effectors within these

pathways, blunting their phenotypic effects. The activation of PI3K signalling *via* the inhibition of PTEN is a powerful pro-regenerative modulation in the ONC axotomy model (Kurimoto et al., 2010; Park et al., 2008). Our statistical overrepresentation analysis implicated miR-340-5p as an important regulator of PI3K activity in neurons, which was confirmed by elevations in pS6 levels in RGCs expressing Circ-340-5p (Fig. 5D, E). While we did not compare these interventions directly, the distance of regenerating fibers observed with Circ-340-5p was less than that reported with *Pten* deletion alone (Park et al., 2008). It is likely that Circ-340-5p elicits a less pronounced effect on PI3K activity than *Pten* deletion alone due to the mixed modulation of both positive and negative effectors within this pathway. In line with this, our *in silico* analysis predicted miR-340-5p regulation of both positive (e.g. *Pdk1*, *Akt*, *mTorC2*) and negative (e.g. *Pten*, *Phlpp*, *Foxo*) effectors within PI3K signalling. Literature evidence has shown that miR-340-5p can enhance PI3K signalling and cell viability by targeting negative effectors of this pathway, such as *Pcd4* (Zheng et al., 2020). In contrast, miR-340-5p inhibits PI3K activation in liver cells *via* targeting of *Ezh2* (Yu et al., 2016), and in the context of osteosarcoma miR-340-5p targets *Lapaatβ* to repress PI3K signalling (Song et al., 2019). Thus, the phenotypic outcome of individual miRNA modulations reflects the complex summation of the regulation of both positive and negative effectors, which can vary between pathways, cell types, and cellular contexts. While Circ-340-5p was able to engage PI3K signalling, it is likely that the targeting of both positive and negative effectors within this pathway diminished this activation when compared to that observed *via* the single deletion of a key switch in the pathway such as *Pten*. Future studies could incorporate miRNA modulations in combination with other robust activators of regeneration to synergistically promote long distance regeneration, neuronal survival, and possible functional recovery of vision.

An important contribution of the current manuscript to the miRNA field is the development and use of a circularized miRNA sponge to promote long-term *in vivo* inhibition of miR-340-5p. Transcribed RNA inhibitors, including those targeting miRNAs, are subject to regular turnover in cells limiting the longevity of their effects (Meister et al., 2004; Nishihara et al., 2013). Additionally, while elevated complementary binding between a target miRNA and its sponge can enhance the sequestration of the miRNA, this can further facilitate the degradation of linear sponge RNA (Ebert and Sharp, 2010). To enhance the longevity and potency of our miR-340-5p sponge, the sponging sequences were flanked between circularization sequences that facilitate back splicing and the formation of 3'-to-5' ligated circular RNA (Liang and Wilusz, 2014). As others have noted, circRNAs are resistant to many of the canonical degradative mechanisms in cells, and thus possess elevated stability (Kristensen et al., 2019; Laveniah et al., 2020). While circularized miRNA sponges hold therapeutic potential for various disease states involving miRNA dysregulation, their synthesis requires optimization based on the choice of intronic or circularization sequences, the complexity of the RNA insert, and the intended delivery mechanism (Choi and Nam, 2024; Meganck et al., 2018; Ron and Ulitsky, 2022).

The trans-species conservation of miRNAs and their target genes is an important consideration when developing miRNA-targeting therapeutics. In this study we focused on miR-340-5p, which has an identical mature sequence in both mice and humans. This conservation increases the likelihood that phenotypes associated with Circ-340-5p will be preserved across species (Friedman et al., 2009). However, a central challenge in miRNA research lies in the extensive range of potential targets and the context-dependent nature of miRNA-mediated gene regulation, which can vary by cell type and physiological state. A more precise understanding of miRNA mechanisms of action will require context-specific, transcriptome-wide analyses of miRNA-target interactions. Recent advances have made this feasible through *in vivo* chimeric miRNA-target sequencing methods such as CLEAR-CLIP, CIMERA-Seq, and related protocols (Grosswendt et al., 2014; Li et al., 2024; Moore et al., 2015). Complementary bioinformatic pipelines

tailored for specific cell types and experimental conditions have also been developed to support these analyses (Mills et al., 2022). High-throughput techniques will ultimately allow for a more comprehensive mapping of the gene networks targeted by individual miRNAs. Notably, Renthal et al. (2020) identified ATF3 as a central transcriptional hub in the DRG conditioning-lesion paradigm, which was not identified as a target of miR-340-5p. In contrast, our goal was to pinpoint factors sufficient, rather than necessary, to drive regeneration, and this difference in focus led us to highlight a different subset of RAGs. Future integration of unbiased, high-throughput approaches will enable a more comprehensive characterization of miRNA-target interactions and may uncover additional layers of miRNA control over key regenerative hubs, thereby deepening our understanding of how miRNAs coordinate axon regeneration and neuronal survival programs.

Our findings demonstrate that miRNA-targeting therapeutics hold significant potential for treating axonal injury by simultaneously modulating numerous gene targets and engaging multiple biological pathways. Circular RNA therapeutics for this purpose can be synthesized with relative ease and offer a means of achieving sustained miRNA inhibition *in vivo*. While the pro-survival effect of Circ-340-5p was not maintained at six weeks post-ONC, regeneration was significantly enhanced between the two- and six-week timepoints, suggesting a sustained regenerative response. Future studies could explore combinatorial strategies that pair this sustained miRNA inhibition with additional pro-survival interventions to further increase the number and extent of regenerating axons in the optic nerve.

CRediT authorship contribution statement

Matthew A. Hintermayer: Writing – review & editing, Writing – original draft, Visualization, Validation, Methodology, Investigation, Formal analysis, Conceptualization. **Elizabeth M.-L. Hua:** Investigation, Data curation. **Mohammed Noor:** Investigation, Formal analysis, Data curation. **Isabel Rambaldi:** Validation, Resources, Methodology, Investigation. **Alyson E. Fournier:** Writing – review & editing, Supervision, Project administration, Funding acquisition, Conceptualization.

Funding sources

A.E.F. is funded by the Canadian Institutes for Health Research and MS Canada. MAH holds a Vanier scholarship from the Canadian Institutes of Health Research (CIHR). E.M.-L.H. holds a master's scholarship from the Fonds de Recherche du Québec-Santé.

Declaration of competing interest

The authors declare no conflicts of interest.

Acknowledgements

The authors thank the Boston Viral core for the packaging and preparation of all AAV2 used in the present manuscript.

Appendix A. Supplementary data

Supplementary data to this article can be found online at <https://doi.org/10.1016/j.expneurol.2025.115527>.

Data availability

Data will be made available on request.

References

- Andrés-León, E., González Peña, D., Gómez-López, G., Pisano, D.G., 2015. miRGate: a curated database of human, mouse and rat miRNA–mRNA targets. Database bav035. <https://doi.org/10.1093/database/bav035>.
- Apara, A., Galvao, J., Wang, Y., Blackmore, M., Trillo, A., Iwao, K., Brown, D.P., Fernandes, K.A., Huang, A., Nguyen, T., Ashouri, M., Zhang, X., Shaw, P.X., Kunzevitzky, N.J., Moore, D.L., Libby, R.T., Goldberg, J.L., 2017. KLF9 and JNK3 interact to suppress axon regeneration in the adult CNS. *J. Neurosci.* 37, 9632–9644. <https://doi.org/10.1523/JNEUROSCI.0643-16.2017>.
- Auricchio, A., Kobinger, G., Anand, V., Hildinger, M., O'Connor, E., Maguire, A.M., Wilson, J.M., Bennett, J., 2001. Exchange of surface proteins impacts on viral vector cellular specificity and transduction characteristics: the retina as a model. *Hum. Mol. Genet.* 10, 3075–3081. <https://doi.org/10.1093/hmg/10.26.3075>.
- Barta, T., Peskova, L., Hampl, A., 2016. miRNAsong: a web-based tool for generation and testing of miRNA sponge constructs in silico. *Sci. Rep.* 6, 36625. <https://doi.org/10.1038/srep36625>.
- Benowitz, L.I., Yin, Y., 2007. Combinatorial treatments for promoting axon regeneration in the CNS: strategies for overcoming inhibitory signals and activating neurons' intrinsic growth state. *Dev. Neurobiol.* 67, 1148–1165. <https://doi.org/10.1002/dneu.20515>.
- Blackmore, M.G., Wang, Z., Lerch, J.K., Motti, D., Zhang, Y.P., Shields, C.B., Lee, J.K., Goldberg, J.L., Lemmon, V.P., Bixby, J.L., 2012. Krüppel-like factor 7 engineered for transcriptional activation promotes axon regeneration in the adult corticospinal tract. *Proc. Natl. Acad. Sci. U. S. A.* 109, 7517–7522. <https://doi.org/10.1073/pnas.1120684109>.
- Cai, J., Grobe, K., Zhang, X., 2014. Role of heparan sulfate proteoglycans in optic disc and stalk morphogenesis. *Dev. Dyn.* 243, 1310–1316. <https://doi.org/10.1002/dvdy.24142>.
- Cameron, E.G., Xia, X., Galvao, J., Ashouri, M., Kapiloff, M.S., Goldberg, J.L., 2020. Optic nerve crush in mice to study retinal ganglion cell survival and regeneration. *Bioprotocol* 10, e3559. <https://doi.org/10.21769/BioProtoc.3559>.
- Chen, H., Weber, A.J., 2001. BDNF enhances retinal ganglion cell survival in cats with optic nerve damage. *Invest. Ophthalmol. Vis. Sci.* 42, 966–974.
- Cheng, L., Sapieha, P., Kittlevá, P., Hauswirth, W.W., Polo, A.D., 2002. TrkB gene transfer protects retinal ganglion cells from axotomy-induced death in vivo. *J. Neurosci.* 22, 3977–3986. <https://doi.org/10.1523/JNEUROSCI.22-10-03977.2002>.
- Choi, S.-W., Nam, J.-W., 2024. Optimal design of synthetic circular RNAs. *Exp. Mol. Med.* 56, 1281–1292. <https://doi.org/10.1038/s12276-024-01251-w>.
- Chou, C.-H., Chang, N.-W., Shrestha, S., Hsu, S.-D., Lin, Y.-L., Lee, W.-H., Yang, C.-D., Hong, H.-C., Wei, T.-Y., Tu, S.-J., Tsai, T.-R., Ho, S.-Y., Jian, T.-Y., Wu, H.-Y., Chen, P.-R., Lin, N.-C., Huang, H.-T., Yang, T.-L., Pai, C.-Y., Tai, C.-S., Chen, W.-L., Huang, C.-Y., Liu, C.-C., Weng, S.-L., Liao, K.-W., Hsu, W.-L., Huang, H.-D., 2016. miRTarBase 2016: updates to the experimentally validated miRNA-target interactions database. *Nucleic Acids Res.* 44, D239–D247. <https://doi.org/10.1093/nar/gkv1258>.
- Cong, M., Li, J., Wang, L., Liu, C., Zheng, M., Zhou, Q., Du, M., Ye, X., Feng, M., Ye, Y., Zhang, S., Xu, W., Lu, Y., Wang, C., Xia, Y., Xie, H., Zhang, Y., He, Q., Gong, L., Gu, Y., Sun, H., Zhang, Q., Zhao, J., Ding, F., Gu, X., Zhou, S., 2024. MicroRNA-25-3p in skin precursor cell-induced Schwann cell-derived extracellular vesicles promotes axon regeneration by targeting Tgf1. *Exp. Neurol.* 376, 114750. <https://doi.org/10.1016/j.exn.2024.114750>.
- Dai, J., Xu, L.-J., Han, G.-D., Sun, H.-L., Zhu, G.-T., Jiang, H.-T., Yu, G.-Y., Tang, X.-M., 2018. MicroRNA-125b promotes the regeneration and repair of spinal cord injury through regulation of JAK/STAT pathway. *Eur. Rev. Med. Pharmacol. Sci.* 22, 582–589. https://doi.org/10.26355/revrem.2018_02_14271.
- Daniel, S., Clark, A.F., McDowell, C.M., 2018. Subtype-specific response of retinal ganglion cells to optic nerve crush. *Cell Death Discov.* 4, 1–16. <https://doi.org/10.1038/s41420-018-0069-y>.
- De Virgiliis, F., Hutson, T.H., Palmisano, I., Amachree, S., Miao, J., Zhou, L., Todorova, R., Thompson, R., Danzi, M.C., Lemmon, V.P., Bixby, J.L., Wittig, I., Shah, A.M., Di Giovanni, S., 2020. Enriched conditioning expands the regenerative ability of sensory neurons after spinal cord injury via neuronal intrinsic redox signaling. *Nat. Commun.* 11, 6425. <https://doi.org/10.1038/s41467-020-20179-z>.
- Di Polo, A., Aigner, L.J., Dunn, R.J., Bray, G.M., Aguayo, A.J., 1998. Prolonged delivery of brain-derived neurotrophic factor by adenovirus-infected Müller cells temporarily rescues injured retinal ganglion cells. *Proc. Natl. Acad. Sci. U. S. A.* 95, 3978–3983. <https://doi.org/10.1073/pnas.95.7.3978>.
- Dubový, P., Klusáková, I., Hradilová-Svíženská, I., Brázda, V., Kohoutková, M., Joukal, M., 2019. A conditioning sciatic nerve lesion triggers a pro-regenerative state in primary sensory neurons also of dorsal root ganglia non-associated with the damaged nerve. *Front. Cell. Neurosci.* 13, 11. <https://doi.org/10.3389/fncel.2019.00011>.
- EBbesen, K.K., Kjems, J., Hansen, T.B., 2016. Circular RNAs: identification, biogenesis and function. *Biochim. Biophys. Acta* 1859, 163–168. <https://doi.org/10.1016/j.bbagr.2015.07.007>.
- Ebert, M.S., Sharp, P.A., 2010. MicroRNA sponges: progress and possibilities. *RNA* 16, 2043–2050. <https://doi.org/10.1261/rna.2414110>.
- Ebert, M.S., Neilson, J.R., Sharp, P.A., 2007. MicroRNA sponges: competitive inhibitors of small RNAs in mammalian cells. *Nat. Methods* 4, 721–726. <https://doi.org/10.1038/nmeth1079>.
- Edwards, T.J., Hammarlund, M., 2014. Syndecan promotes axon regeneration by stabilizing growth cone migration. *Cell Rep.* 8, 272–283. <https://doi.org/10.1016/j.celrep.2014.06.008>.
- Feng, L., Puyang, Z., Chen, H., Liang, P., Troy, J.B., Liu, X., 2017. Overexpression of brain-derived neurotrophic factor protects large retinal ganglion cells after optic nerve crush in mice. *eNeuro* 4, ENEURO.0331-16.2016. <https://doi.org/10.1523/ENEURO.0331-16.2016>.
- Feng, Q., Wang, H., Shao, Y., Xu, X., 2024. Antizyme inhibitor family: biological and translational research implications. *Cell Communication and Signaling* 22, 11. <https://doi.org/10.1186/s12964-023-01445-1>.
- Friedman, R.C., Farh, K.K.-H., Burge, C.B., Bartel, D.P., 2009. Most mammalian mRNAs are conserved targets of microRNAs. *Genome Res.* 19, 92–105. <https://doi.org/10.1101/gr.082701.108>.
- Gaudet, A.D., Mandrekar-Colucci, S., Hall, J.C.E., Sweet, D.R., Schmitt, P.J., Xu, X., Guan, Z., Mo, X., Guerau-de-Arellano, M., Popovich, P.G., 2016. miR-155 deletion in mice overcomes neuron-intrinsic and neuron-extrinsic barriers to spinal cord repair. *J. Neurosci.* 36, 8516–8532. <https://doi.org/10.1523/JNEUROSCI.0735-16.2016>.
- Gilad, G.M., Gilad, V.H., 1983. Early rapid and transient increase in ornithine decarboxylase activity within sympathetic neurons after axonal injury. *Exp. Neurol.* 81, 158–166. [https://doi.org/10.1016/0014-4886\(83\)90165-6](https://doi.org/10.1016/0014-4886(83)90165-6).
- Grosswendt, S., Filipchik, A., Manzano, M., Kliromos, F., Schilling, M., Herzog, M., Gottwein, E., Rajewsky, N., 2014. Unambiguous identification of miRNA:target site interactions by different types of ligation reactions. *Mol. Cell* 54, 1042–1054. <https://doi.org/10.1016/j.molcel.2014.03.049>.
- Guo, H., Ingolia, N.T., Weissman, J.S., Bartel, D.P., 2010. Mammalian microRNAs predominantly act to decrease target mRNA levels. *Nature* 466, 835–840. <https://doi.org/10.1038/nature09267>.
- Han, F., Huo, Y., Huang, C.-J., Chen, C.-L., Ye, J., 2015. MicroRNA-30b promotes axon outgrowth of retinal ganglion cells by inhibiting Semaphorin3A expression. *Brain Res.* 1611, 65–73. <https://doi.org/10.1016/j.brainres.2015.03.014>.
- Hancock, M.L., Preitner, N., Quan, J., Flanagan, J.G., 2014. MicroRNA-132 is enriched in developing axons, locally regulates Rasa1 mRNA, and promotes axon extension. *J. Neurosci.* 34, 66–78. <https://doi.org/10.1523/JNEUROSCI.3371-13.2014>.
- Hay, N., Sonnenberg, N., 2004. Upstream and downstream of mTOR. *Genes Dev.* 18, 1926–1945. <https://doi.org/10.1101/gad.1212704>.
- He, M., Liu, Y., Wang, X., Zhang, M.Q., Hannon, G., Huang, Z.J., 2012. Cell-type based analysis of microRNA profiles in the mouse brain. *Neuron* 73, 35–48. <https://doi.org/10.1016/j.neuron.2011.11.010>.
- Hintermayer, M.A., Južník, C.A., Morquette, B., Hua, E., Zhang, J., Drake, S., Shi, S.S., Rambaldi, I., Vangoor, V., Pasterkamp, J., Moore, C., Fournier, A.E., 2024. A miR-383-5p Signaling hub coordinates the axon regeneration response to inflammation. *J. Neurosci.* 44. <https://doi.org/10.1523/JNEUROSCI.1822-23.2024>.
- Hoye, M.L., Koval, E.D., Wegener, A.J., Hyman, T.S., Yang, C., O'Brien, D.R., Miller, R.L., Cole, T., Schoch, K.M., Shen, T., Kumikata, T., Richard, J.-P., Gutmann, D.H., Maragakis, N.J., Kordasiewicz, H.B., Dougherty, J.D., Miller, T.M., 2017. MicroRNA profiling reveals marker of motor neuron disease in ALS models. *J. Neurosci.* 37, 5574–5586. <https://doi.org/10.1523/JNEUROSCI.3582-16.2017>.
- Hu, G., Huang, K., Hu, Y., Du, G., Xue, Z., Zhu, X., Fan, G., 2016. Single-cell RNA-seq reveals distinct injury responses in different types of DRG sensory neurons. *Sci. Rep.* 6, 31851. <https://doi.org/10.1038/srep31851>.
- Huang, H.-Y., Lin, Y.-C.-D., Cui, S., Huang, Y., Tang, Y., Xu, J., Bao, J., Li, Y., Wen, J., Zuo, H., Wang, W., Li, J., Ni, J., Ruan, Y., Li, L., Chen, Yidan, Xie, Y., Zhu, Z., Cai, X., Chen, X., Yao, L., Chen, Yigang, Luo, Y., LuXu, S., Luo, M., Chiu, C.-M., Ma, K., Zhu, L., Cheng, G.-J., Bai, C., Chiang, Y.-C., Wang, L., Wei, F., Lee, T.-Y., Huang, H.-D., 2022. miRTarBase update 2022: an informative resource for experimentally validated miRNA-target interactions. *Nucleic Acids Res.* 50, D222–D230. <https://doi.org/10.1093/nar/gkab1079>.
- Kadoya, K., Tsukada, S., Lu, P., Coppola, G., Geschwind, D., Filbin, M.T., Blesch, A., Tuszyński, M.H., 2009. Combined intrinsic and extrinsic neuronal mechanisms facilitate bridging axonal regeneration one year after spinal cord injury. *Neuron* 64, 165–172. <https://doi.org/10.1016/j.neuron.2009.09.016>.
- Kanaizumi, H., Higashi, C., Tanaka, Y., Hamada, M., Shinzaki, W., Azumi, T., Hashimoto, Y., Inui, H., Houjou, T., Komoike, Y., 2018. PI3K/Akt/mTOR signalling pathway activation in patients with ER-positive, metachronous, contralateral breast cancer treated with hormone therapy. *Oncol. Lett.* 17, 1962. <https://doi.org/10.3892/ol.2018.9759>.
- Kluiver, J., Gibcus, J.H., Hettinga, C., Adema, A., Richter, M.K.S., Halsema, N., Slezak-Prochazka, I., Ding, Y., Kroesen, B.-J., van den Berg, A., 2012a. Rapid generation of microRNA sponges for microRNA inhibition. *PloS One* 7, e29275. <https://doi.org/10.1371/journal.pone.0029275>.
- Kluiver, J., Slezak-Prochazka, I., Smigelska-Czepiel, K., Halsema, N., Kroesen, B.-J., van den Berg, A., 2012b. Generation of miRNA sponge constructs. *Methods* 58, 113–117. <https://doi.org/10.1016/j.ymeth.2012.07.019>.
- Kozomara, A., Birgaoanu, M., Griffiths-Jones, S., 2019. miRBase: from microRNA sequences to function. *Nucleic Acids Res.* 47, D155–D162. <https://doi.org/10.1093/nar/gky1141>.
- Kristensen, L.S., Andersen, M.S., Stagsted, L.V.W., Ebbesen, K.K., Hansen, T.B., Kjems, J., 2019. The biogenesis, biology and characterization of circular RNAs. *Nat. Rev. Genet.* 20, 675–691. <https://doi.org/10.1038/s41576-019-0158-7>.
- Kurimoto, T., Yin, Y., Omura, K., Gilbert, H., Kim, D., Cen, L.-P., Moko, L., Kübler, S., Benowitz, L.I., 2010. Long-distance axon regeneration in the mature optic nerve: contributions of oncomodulin, cAMP, and pten gene deletion. *J. Neurosci.* 30, 15654–15663. <https://doi.org/10.1523/JNEUROSCI.4340-10.2010>.
- Labisch, J.J., Wiese, G.P., Barnes, K., Bollmann, F., Pflanz, K., 2021. Infectious titer determination of lentiviral vectors using a temporal immunological real-time imaging approach. *PLoS One* 16, e0254739. <https://doi.org/10.1371/journal.pone.0254739>.
- Lavenniah, A., Luu, T.D.A., Li, Y.P., Lim, T.B., Jiang, J., Ackers-Johnson, M., Foo, R.S.-Y., 2020. Engineered circular RNA sponges act as miRNA inhibitors to attenuate

- pressure overload-induced cardiac hypertrophy. *Mol. Ther.* 28, 1506–1517. <https://doi.org/10.1016/j.ymthe.2020.04.006>.
- Leon, S., Yin, Y., Nguyen, J., Irwin, N., Benowitz, L.I., 2000. Lens injury stimulates axon regeneration in the mature rat optic nerve. *J. Neurosci.* 20, 4615–4626.
- Lewis, B.P., Shih, I., Jones Rhoades, M.W., Bartel, D.P., Burge, C.B., 2003. Prediction of mammalian microRNA targets. *Cell* 115, 787–798. [https://doi.org/10.1016/s0092-8674\(03\)01018-3](https://doi.org/10.1016/s0092-8674(03)01018-3).
- Lewis, B.P., Burge, C.B., Bartel, D.P., 2005. Conserved seed pairing, often flanked by adenosines, indicates that thousands of human genes are microRNA targets. *Cell* 120, 15–20. <https://doi.org/10.1016/j.cell.2004.12.035>.
- Li, H., Yang, B.B., 2013. Friend or foe: the role of microRNA in chemotherapy resistance. *Acta Pharmacol. Sin.* 34, 870–879. <https://doi.org/10.1038/aps.2013.35>.
- Li, X., Mills, W.T., Jin, D.S., Meffert, M.K., 2024. Genome-wide and cell-type-selective profiling of *in vivo* small noncoding RNA:target RNA interactions by chimeric RNA sequencing. *Cell Rep Methods* 4, 100836. <https://doi.org/10.1016/j.crm.2024.100836>.
- Liang, D., Wilusz, J.E., 2014. Short intronic repeat sequences facilitate circular RNA production. *Genes Dev.* 28, 2233–2247. <https://doi.org/10.1101/gad.251926.114>.
- Liú, C.-M., Wang, R.-Y., Sajilalifa Jiao, Z.-X., Zhang, B.Y., Zhou, F.-Q., 2013. MicroRNA-138 and SIRT1 form a mutual negative feedback loop to regulate mammalian axon regeneration. *Genes Dev.* 27, 1473. <https://doi.org/10.1101/gad.209619.112>.
- Lu, X.C., Zheng, J.Y., Tang, L.J., Huang, B.S., Li, K., Tao, Y., Yu, W., Zhu, R.L., Li, S., Li, L.X., 2015. MiR-133b promotes neurite outgrowth by targeting RhoA expression. *Cell. Physiol. Biochem.* 35, 246–258. <https://doi.org/10.1159/000369692>.
- Lukomska, A., Theune, W.C., Frost, M.P., Xing, J., Kearney, A., Trakhtenberg, E.F., 2024. Upregulation of developmentally-downregulated miR-1247-5p promotes neuroprotection and axon regeneration *in vivo*. *Neurosci. Lett.* 823, 137662. <https://doi.org/10.1016/j.neulet.2024.137662>.
- Mak, H.K., Yung, J.S.Y., Weinreb, R.N., Ng, S.H., Cao, X., Ho, T.Y.C., Ng, T.K., Chu, W.K., Yung, W.H., Choy, K.W., Wang, C.C., Lee, T.L., Leung, C.K., 2020. MicroRNA-19a-PTEN Axis is involved in the developmental decline of axon regenerative capacity in retinal ganglion cells. *Mol Ther Nucleic Acids* 21, 251–263. <https://doi.org/10.1016/j.mtn.2020.05.031>.
- McQuarrie, I.G., Grafstein, B., 1973. Axon outgrowth enhanced by a previous nerve injury. *Arch. Neurol.* 29, 53–55. <https://doi.org/10.1001/archneur.1973.00490250071008>.
- Mead, B., Kerr, A., Nakaya, N., Tomarev, S.I., 2021. miRNA changes in retinal ganglion cells after optic nerve crush and glaucomatous damage. *Cells* 10, 1564. <https://doi.org/10.3390/cells10071564>.
- Meganck, R.M., Borchardt, E.K., Castellanos Rivera, R.M., Scalabrino, M.L., Wilusz, J.E., Marzluff, W.F., Asokan, A., 2018. Tissue-dependent expression and translation of circular RNAs with recombinant AAV vectors *in vivo*. *Mol Ther Nucleic Acids* 13, 89–98. <https://doi.org/10.1016/j.omtn.2018.08.008>.
- Meister, G., Landthaler, M., Dorsett, Y., Tuschl, T., 2004. Sequence-specific inhibition of microRNA- and siRNA-induced RNA silencing. *RNA* 10, 544. <https://doi.org/10.1261/rna.5235104>.
- Mills, W.T., Eadarra, S., Jaffe, A.E., Meffert, M.K., 2022. SCRAP: a bioinformatic pipeline for the analysis of small chimeric RNA-seq data. *RNA* 29, 1–17. <https://doi.org/10.1261/ma.079240.122>.
- Missaghian, P., Dierker, T., Khosrowabadi, E., Axling, F., Eriksson, I., Ghanem, A., Kusche-Gullberg, M., Kellokumpu, S., Kjellén, L., 2022. A dominant negative splice variant of the heparan sulfate biosynthesis enzyme NDST1 reduces heparan sulfate sulfation. *Glycobiology* 32, 518–528. <https://doi.org/10.1093/glycob/cwac004>.
- Momin, M.Y., Gaddam, R.R., Kravitz, M., Gupta, A., Vikram, A., 2021. The challenges and opportunities in the development of MicroRNA therapeutics: multidisciplinary viewpoint. *Cells* 10, 3097. <https://doi.org/10.3390/cells10113097>.
- Moore, D.L., Blackmore, M.G., Hu, Y., Kaestner, K.H., Bibby, J.L., Lemmon, V.P., Goldberg, J.L., 2009. KLF family members regulate intrinsic axon regeneration ability. *Science* 326, 298–301. <https://doi.org/10.1126/science.1175737>.
- Moore, M.J., Scheel, T.K.H., Luna, J.M., Park, C.Y., Fak, J.J., Nishiuchi, E., Rice, C.M., Darnell, R.B., 2015. miRNA-target chimeras reveal miRNA 3'-end pairing as a major determinant of Argonaute target specificity. *Nat. Commun.* 6, 8864. <https://doi.org/10.1038/ncomms9864>.
- Murakami, K., Tanaka, T., Bando, Y., Yoshida, S., 2015. Nerve injury induces the expression of syndecan-1 heparan sulfate proteoglycan in primary sensory neurons. *Neuroscience* 300, 338–350. <https://doi.org/10.1016/j.neuroscience.2015.05.033>.
- Nampoothiri, S.S., Rajanikant, G.K., 2019. miR-9 upregulation integrates post-ischemic neuronal survival and regeneration *in vitro*. *Cell. Mol. Neurobiol.* 39, 223–240. <https://doi.org/10.1007/s10571-018-0642-1>.
- Neumann, S., Woolf, C.J., 1999. Regeneration of dorsal column fibers into and beyond the lesion site following adult spinal cord injury. *Neuron* 23, 83–91. [https://doi.org/10.1016/s0896-6273\(00\)80755-2](https://doi.org/10.1016/s0896-6273(00)80755-2).
- Niemi, J.P., DeFrancesco-Oranburg, T., Cox, A., Lindborg, J.A., Echevarria, F.D., McCluskey, J., Simmons, D.D., Zigmond, R.E., 2022. The Conditioning Lesion Response in Dorsal Root Ganglion Neurons Is Inhibited in Oncomodulin Knock-out Mice, vol. eNeuro 9, eNEURO.0477-21.2022. <https://doi.org/10.1523/ENEURO.0477-21.2022>.
- Nishihara, T., Zekri, L., Braun, J.E., Izaurralde, E., 2013. miRISC recruits decapping factors to miRNA targets to enhance their degradation. *Nucleic Acids Res.* 41, 8692–8705. <https://doi.org/10.1093/nar/gkt619>.
- Noro, T., Namekata, K., Kimura, A., Guo, X., Azuchi, Y., Harada, C., Nakano, T., Tsuneoka, H., Harada, T., 2015. Spermidine promotes retinal ganglion cell survival and optic nerve regeneration in adult mice following optic nerve injury. *Cell Death Dis.* 6, e1720. <https://doi.org/10.1038/cddis.2015.93>.
- Ohtake, Y., Hayat, U., Li, S., 2015. PTEN inhibition and axon regeneration and neural repair. *Neural Regen. Res.* 10, 1363–1368. <https://doi.org/10.4103/1673-5374.165496>.
- Olsen, R.R., Zetter, B.R., 2011. Evidence of a role for antizyme and antizyme inhibitor as regulators of human cancer. *Mol. Cancer Res.* 9, 1285–1293. <https://doi.org/10.1158/1541-7786.MCR-11-0178>.
- Pan, Y., Woodbury, A., Esko, J.D., Grobe, K., Zhang, X., 2006. Heparan sulfate biosynthetic gene Ndst1 is required for FGF signaling in early lens development. *Development* 133, 4933–4944. <https://doi.org/10.1242/dev.02679>.
- Panda, A.C., 2018. Circular RNAs act as miRNA sponges. *Adv. Exp. Med. Biol.* 1087, 67–79. https://doi.org/10.1007/978-981-13-1426-1_6.
- Pang, J., Lauramore, A., Deng, W., Li, Q., Doyle, T.J., Chioldo, V., Li, J., Hauswirth, W.W., 2008. Comparative analysis of *in vivo* and *in vitro* AAV vector transduction in the neonatal mouse retina: effects of serotype and site of administration. *Vision Res.* 48, 377–385. <https://doi.org/10.1016/j.visres.2007.08.009>.
- Paré, A., Mailhot, B., Lévesque, S.A., Juzwik, C., Ignatius Arokia Doss, P.M., Lécuyer, M.-A., Prat, A., Rangachari, M., Fournier, A., Lacroix, S., 2018. IL-1 β enables CNS access to CCR2hi monocytes and the generation of pathogenic cells through GM-CSF released by CNS endothelial cells. *Proc. Natl. Acad. Sci. U. S. A.* 115, E1194–E1203. <https://doi.org/10.1073/pnas.1714948115>.
- Park, K.K., Liu, K., Hu, Y., Smith, P.D., Wang, C., Cai, B., Xu, B., Connolly, L., Kramvis, I., Sahin, M., He, Z., 2008. Promoting axon regeneration in the adult CNS by modulation of the PTEN/mTOR pathway. *Science* 322, 963–966. <https://doi.org/10.1126/science.1161566>.
- Phay, M., Kim, H.H., Yoo, S., 2015. Dynamic change and target prediction of axon-specific MicroRNAs in regenerating sciatic nerve. *PLoS One* 10, e0137461. <https://doi.org/10.1371/journal.pone.0137461>.
- Pomper, N., Liu, Y., Hoye, M.L., Dougherty, J.D., Miller, T.M., 2020. CNS microRNA profiles: a database for cell type enriched microRNA expression across the mouse central nervous system. *Sci Rep* 10, 4921. <https://doi.org/10.1038/s41598-020-61307-5>.
- Puttagunta, R., Tedeschi, A., Sória, M.G., Hervera, A., Lindner, R., Rathore, K.I., Gaub, P., Joshi, Y., Nguyen, T., Schmandke, A., Laskowski, C.J., Boutillier, A.-L., Bradke, F., Di Giovanni, S., 2014. PCAF-dependent epigenetic changes promote axonal regeneration in the central nervous system. *Nat. Commun.* 5, 3527. <https://doi.org/10.1038/ncomms4527>.
- Qin, T., Li, C., Xu, Y., Qin, Y., Jin, Y., He, R., Luo, Z., Zhao, J., Duan, C., Lu, H., Cao, Y., Hu, J., 2023. Local delivery of EGFR+NSCs-derived exosomes promotes neural regeneration post spinal cord injury via miR-34a-5p/HDAC6 pathway. *Bioactive Materials* 33, 424. <https://doi.org/10.1016/j.bioactmat.2023.11.013>.
- Raines, A.N., Nagdas, S., Kerber, M.L., Cheney, R.E., 2012. Headless Myo10 is a negative regulator of full-length Myo10 and inhibits axon outgrowth in cortical neurons. *J. Biol. Chem.* 287, 24873–24883. <https://doi.org/10.1074/jbc.M112.369173>.
- Rasmussen, S., Roberts, P., 2007. Functional studies of microRNA based on knockdown using locked nucleic acid probes. *Nat. Methods* 4, iii–iv. <https://doi.org/10.1038/nmeth1034>.
- Renthal, W., Tochitsky, I., Yang, L., Cheng, Y.-C., Li, E., Kawaguchi, R., Geschwind, D.H., Woolf, C.J., 2020. Transcriptional reprogramming of distinct peripheral sensory neuron subtypes after axonal injury. *Neuron* 108, 128–144.e9. <https://doi.org/10.1016/j.neuron.2020.07.026>.
- Ron, M., Ulitsky, I., 2022. Context-specific effects of sequence elements on subcellular localization of linear and circular RNAs. *Nat. Commun.* 13, 2481. <https://doi.org/10.1038/s41467-022-30183-0>.
- Shishioh, N., Kiryu-Seo, S., Abe-Dohmae, S., Yokoyama, S., Kiyama, H., 2022. Expression of ATP-binding cassette transporter A1 is induced by nerve injury and its deficiency affects neurite tip morphology and elongation in cultured neurons. *J. Chem. Neuroanat.* 125, 102164. <https://doi.org/10.1016/j.jchemneu.2022.102164>.
- Song, L., Zhou, Z., Gan, Y., Li, P., Xu, Y., Zhang, Z., Luo, F., Xu, J., Zhou, Q., Dai, F., 2019. Long noncoding RNA OIP5-AS1 causes cisplatin resistance in osteosarcoma through inducing the LPAAT β /PI3K/AKT/mTOR signaling pathway by sponging the miR-340-5p. *J. Cell. Biochem.* 120, 9656–9666. <https://doi.org/10.1002/jcb.28244>.
- Strickland, I.T., Richards, L., Holmes, F.E., Wynick, D., Uney, J.B., Wong, L.-F., 2011. Axotomy-induced miR-21 promotes axon growth in adult dorsal root ganglion neurons. *PLoS One* 6, e23423. <https://doi.org/10.1371/journal.pone.0023423>.
- Su, H., Xiaohui, X., He, X., Liu, C., Wang, G., Zhou, C., 2020. The miR-455-5p/miR-455 axis regulates mammalian neuronal viability and axonal regeneration. *Neurosci. Lett.* 735, 135159. <https://doi.org/10.1016/j.neulet.2020.135159>.
- Sun, F., Park, K.K., Belin, S., Wang, D., Lu, T., Chen, G., Zhang, K., Yeung, C., Feng, G., Yankner, B.A., He, Z., 2011. Sustained axon regeneration induced by co-deletion of PTEN and SOCS3. *Nature* 480, 372–375. <https://doi.org/10.1038/nature10594>.
- Szklarczyk, D., Kirsch, R., Koutrouli, M., Nastou, K., Mehryary, F., Hachilif, R., Gable, A., L., Fang, T., Doncheva, N.T., Pyysalo, S., Bork, P., Jensen, L.J., von Mering, C., 2023. The STRING database in 2023: protein-protein association networks and functional enrichment analyses for any sequenced genome of interest. *Nucleic Acids Res.* 51, D638–D646. <https://doi.org/10.1093/nar/gkac1000>.
- Tanabe, K., Bonilla, I., Winkles, J.A., Strittmatter, S.M., 2003. Fibroblast growth factor-Inducible-14 is induced in axotomized neurons and promotes neurite outgrowth. *J. Neurosci.* 23, 9675–9686. <https://doi.org/10.1523/JNEUROSCI.23-29-09675-2003>.
- Tang, Y., Garson, K., Li, L., Vanderhyden, B.C., 2015. Optimization of lentiviral vector production using polyethylenimine-mediated transfection. *Oncol. Lett.* 9, 55–62. <https://doi.org/10.3892/ol.2014.2684>.
- Taniguchi, T., Sharif, N.A., Ota, T., Farjo, R.A., Rausch, R., 2024. Assessment of brain-derived neurotrophic factor on retinal structure and visual function in rodent models of optic nerve crush. *Pharmaceuticals (Basel)* 17, 798. <https://doi.org/10.3390/ph17060798>.

- Tedeschi, A., Bradke, F., 2017. Spatial and temporal arrangement of neuronal intrinsic and extrinsic mechanisms controlling axon regeneration. *Current Opinion in Neurobiology* 42, 118–127. <https://doi.org/10.1016/j.conb.2016.12.005>.
- Tetzlaff, W., Kreutzberg, G.W., 1985. Ornithine decarboxylase in motoneurons during regeneration. *Exp. Neurol.* 89, 679–688. [https://doi.org/10.1016/0014-4886\(85\)90016-0](https://doi.org/10.1016/0014-4886(85)90016-0).
- Tran, N.M., Shekhar, K., Whitney, I.E., Jacobi, A., Benhar, I., Hong, G., Yan, W., Adiconis, X., Arnold, M.E., Lee, J.M., Levin, J.Z., Lin, D., Wang, C., Lieber, C.M., Regev, A., He, Z., Sanes, J.R., 2019. Single-cell profiles of retinal ganglion cells differing in resilience to injury reveal neuroprotective genes. *Neuron* 104, 1039–1055.e12. <https://doi.org/10.1016/j.neuron.2019.11.006>.
- van Battum, E.Y., Verhagen, M.G., Vangoor, V.R., Fujita, Y., Derijck, A.A.H.A., O'Duibhir, E., Giuliani, G., de Gunst, T., Adolfs, Y., Lelieveld, D., Egan, D., Schaapveld, R.Q.J., Yamashita, T., Pasterkamp, R.J., 2018. An image-based miRNA screen identifies miRNA-135s as regulators of CNS axon growth and regeneration by targeting Krüppel-like factor 4. *J. Neurosci.* 38, 613–630. <https://doi.org/10.1523/JNEUROSCI.0662-17.2017>.
- Vidal-Villegas, B., Di Pierdomenico, J., Gallego-Ortega, A., Galindo-Romero, C., Martínez-de-la-Casa, J.M., García-Feijoo, J., Villegas-Pérez, M.P., Vidal-Sanz, M., 2021. Systemic treatment with 7,8-Dihydroxiflavone activates Ttk8 and affords protection of two different retinal ganglion cell populations against axotomy in adult rats. *Exp. Eye Res.* 210, 108694. <https://doi.org/10.1016/j.exer.2021.108694>.
- Wang, T., Li, B., Wang, Z., Yuan, X., Chen, C., Zhang, Y., Xia, Z., Wang, Xin, Yu, M., Tao, W., Zhang, L., Wang, Xu, Zhang, Z., Guo, X., Ning, G., Feng, S., Chen, X., 2019. miR-155-5p promotes dorsal root ganglion neuron axonal growth in an inhibitory microenvironment via the cAMP/PKA pathway. *Int. J. Biol. Sci.* 15, 1557–1570. <https://doi.org/10.7150/ijbs.31904>.
- Wang, N., Yang, Y., Pang, M., Du, C., Chen, Y., Li, S., Tian, Z., Feng, F., Wang, Y., Chen, Z., Liu, B., Rong, L., 2020. MicroRNA-135a-5p promotes the functional recovery of spinal cord injury by targeting SP1 and ROCK. *Mol Ther Nucleic Acids* 22, 1063–1077. <https://doi.org/10.1016/j.mtn.2020.08.035>.
- Wang, C., Ji, Y., Zhang, H., Ye, Y., Zhang, G., Zhang, S., Zhao, C., Wang, Y., 2023. Increased level of exosomal miR-20b-5p derived from hypothermia-treated microglia promotes neurite outgrowth and synapse recovery after traumatic brain injury. *Neurobiol. Dis.* 179, 106042. <https://doi.org/10.1016/j.nbd.2023.106042>.
- Wells, M.R., 1987. Changes of ornithine decarboxylase activity in dorsal root ganglion cells after axon injury: possible relationship to alterations in neuronal chromatin. *Exp. Neurol.* 95, 313–322. [https://doi.org/10.1016/0014-4886\(87\)90141-5](https://doi.org/10.1016/0014-4886(87)90141-5).
- White, R.E., Giffard, R.G., 2012. MicroRNA-320 induces neurite outgrowth by targeting ARPP-19. *Neuroreport* 23, 590–595. <https://doi.org/10.1097/WNR.0b013e3283540394>.
- Wu, D., Raafat, A., Pak, E., Clemens, S., Murashov, A.K., 2012. Dicer-microRNA pathway is critical for peripheral nerve regeneration and functional recovery in vivo and regenerative axonogenesis in vitro. *Exp. Neurol.* 233, 555–565. <https://doi.org/10.1016/j.expneurol.2011.11.041>.
- Xiao, J., Joseph, S., Xia, M., Teng, F., Chen, X., Huang, R., Zhai, L., Deng, W., 2022. Circular RNAs acting as miRNAs' sponges and their roles in stem cells. *J. Clin. Med.* 11, 2909. <https://doi.org/10.3390/jcm11102909>.
- Yang, S.-G., Li, C.-P., Peng, X.-Q., Teng, Z.-Q., Liu, C.-M., Zhou, F.-Q., 2020. Strategies to promote long-distance optic nerve regeneration. *Front. Cell. Neurosci.* 14.
- Yang, J., Chen, Y., Zou, T., Xue, B., Yang, F., Wang, X., Huo, Y., Yan, B., Xu, Y., He, S., Yin, Y., Wang, J., Zhu, Xiong, Zhang, L., Zhou, Y., Tai, Z., Shuai, P., Yu, M., Luo, Q., Cheng, Y., Gong, B., Zhu, Xianjun, Zhang, J., Sun, X., Lin, Y., Zhang, H., Yang, Z., 2023. Cholesterol homeostasis regulated by ABCA1 is critical for retinal ganglion cell survival. *Sci. China Life Sci.* 66, 211–225. <https://doi.org/10.1007/s11427-021-2126-2>.
- Yu, Y.-M., Gibbs, K.M., Davila, J., Campbell, N., Sung, S., Todorova, T.I., Otsuka, S., Sabaaawy, H.E., Hart, R.P., Schachner, M., 2011. MicroRNA miR-133b is essential for functional recovery after spinal cord injury in adult zebrafish. *Eur. J. Neurosci.* 33, 1587–1597. <https://doi.org/10.1111/j.1460-9568.2011.07643.x>.
- Yu, H., Wang, N., Ju, X., Yang, Y., Sun, D., Lai, M., Cui, L., Sheikh, M.A., Zhang, J., Wang, X., Zhu, X., 2012. PtdIns (3,4,5) P3 recruitment of Myo10 is essential for axon development. *PloS One* 7, e36988. <https://doi.org/10.1371/journal.pone.0036988>.
- Yu, W., Zhang, G., Lu, B., Li, J., Wu, Z., Ma, H., Wang, H., Lian, R., 2016. MiR-340 impedes the progression of laryngeal squamous cell carcinoma by targeting EZH2. *Gene* 577, 193–201. <https://doi.org/10.1016/j.gene.2015.11.045>.
- Zhang, Jun, Zhang, Jing, Liu, L., Zhou, Y., Li, Y., Shao, Z., Wu, Y., Li, M., Fan, Y., Shi, H., 2011. Effects of miR-541 on neurite outgrowth during neuronal differentiation. *Cell Biochem. Funct.* 29, 279–286. <https://doi.org/10.1002/cbf.1747>.
- Zhang, Y., Williams, P.R., Jacobi, A., Wang, C., Goel, A., Hirano, A.A., Brecha, N.C., Kerschensteiner, D., He, Z., 2019. Elevating growth factor responsiveness and axon regeneration by modulating presynaptic inputs. *Neuron* 103, 39–51.e5. <https://doi.org/10.1016/j.neuron.2019.04.033>.
- Zhang, N., Lin, J., Chin, J.S., Zhang, K., Chew, S.Y., 2020a. A laser microdissection-based axotomy model incorporating the use of biomimicking fiber scaffolds reveals that microRNAs promote axon regeneration over long injury distances. *Biomater. Sci.* 8, 6286–6300. <https://doi.org/10.1039/DOBM01380C>.
- Zhang, L., Wang, Z., Li, B., Xia, Z., Wang, X., Xiu, Y., Zhang, Z., Chen, C., Song, H., Li, W., Yu, M., Zhang, M., Wang, K., Guo, X., Ren, L., Wang, T., 2020b. The inhibition of miR-17-5p promotes cortical neuron neurite growth via STAT3/GAP-43 pathway. *Mol. Biol. Rep.* 47, 1795–1802. <https://doi.org/10.1007/s11033-020-05273-1>.
- Zhao, L., Gong, L., Li, P., Qin, J., Xu, L., Wei, Q., Xie, H., Mao, S., Yu, B., Gu, X., Zhou, S., 2021. miR-20a promotes the axon regeneration of DRG neurons by targeting Nr4a3. *Neurosci. Bull.* 37, 569–574. <https://doi.org/10.1007/s12264-021-00647-2>.
- Zhao, L.-L., Zhang, T., Huang, W.-X., Guo, T.-T., Gu, X.-S., 2023. Transcriptional regulatory network during axonal regeneration of dorsal root ganglion neurons: laser-capture microdissection and deep sequencing. *Neural Regen. Res.* 18, 2056. <https://doi.org/10.4103/1673-5374.366494>.
- Zheng, Y., Zhao, P., Lian, Y., Li, S., Chen, Y., Li, L., 2020. MiR-340-5p alleviates oxygen-glucose deprivation/reoxygenation-induced neuronal injury via PI3K/Akt activation by targeting PDCD4. *Neurochem. Int.* 134, 104650. <https://doi.org/10.1016/j.neuint.2019.104650>.
- Zhou, W.-Y., Cai, Z.-R., Liu, J., Wang, D.-S., Ju, H.-Q., Xu, R.-H., 2020. Circular RNA: metabolism, functions and interactions with proteins. *Mol. Cancer* 19, 172. <https://doi.org/10.1186/s12943-020-01286-3>.
- Zhu, X.-J., Wang, C.-Z., Dai, P.-G., Xie, Y., Song, N.-N., Liu, Y., Du, Q.-S., Mei, L., Ding, Y.-Q., Xiong, W.-C., 2007. Myosin X regulates netrin receptors and functions in axonal path-finding. *Nat. Cell Biol.* 9, 184–192. <https://doi.org/10.1038/ncb1535>.
- Zhu, J., Li, Q., Wu, Z., Xu, W., Jiang, R., 2024. Circular RNA-mediated miRNA sponge & RNA binding protein in biological modulation of breast cancer. *Non-coding RNA Res.* 9, 262–276. <https://doi.org/10.1016/j.ncrna.2023.12.005>.